الجمهورية الجزائرية الديمقراطية الشعبية
THE PEOPLE'S DEMOCRATIC REPUBLIC OF ALGERIA
وزارة التعليم العالي و البحث العلمي
THE MINISTRY OF HIGHER EDUCATION AND SCIENTIFIC RESEARCH
جامعة عمّار ثليجي بالأغواط
AMAR TELIDJI UNIVERSITY OF LAGHOUAT
كلية التكنولوجيا
FACULTY OF TECHNOLOGY
قسم الالكتروتقني
DEPARTMENT OF ELECTROTECHNIC

Master's Dissertation

Domain: Science and Technology
Field: Electrical Engineering
Option: Automation and Systems

Presented by:
LAGGOUN SAFA MALAK and NEKKAR MELISSA

THEME

Motor Torque Estimation and Security Control for Electric Vehicle Applications

Jury Members:

Abderezzak Hadjer	MCB	President
Ameur Iyad	MCB	Examiner
D. Bengjedia Bachir	MCA	Supervisor
M. Bougrine Djameleddine	MCB	Co-Supervisor

Academic Year 2025/2026

Abstract

Abstract

Electric vehicle (EV) propulsion systems require high-performance control strategies to ensure accurate speed regulation and robustness against external disturbances. Among the factors affecting drive performance, load torque variations caused by road conditions, vehicle mass changes, and resistive forces can significantly degrade speed tracking and dynamic response.

This thesis investigates the use of observer-based load torque estimation techniques to enhance the performance of a DC motor drive intended for electric vehicle applications. Three estimation methods are studied: the Luenberger Observer (LO), Sliding Mode Observer (SMO), and Extended State Observer (ESO). Their mathematical formulations are developed and their estimation capabilities are first evaluated under open-loop conditions.

The proposed observers are then integrated into a closed-loop speed control system, and their performance is assessed through simulation under various operating conditions. Finally, the developed approach is applied to a 1.5 kW DC motor-based electric vehicle propulsion system. The results demonstrate that accurate load torque estimation improves disturbance rejection, speed tracking performance, and overall system robustness.

Keywords: Electric Vehicle, DC Motor Drive, Load Torque Estimation, Luenberger Observer, Sliding Mode Observer, Extended State Observer, ADRC, Speed Control.

يركز هذا العمل على نمذجة والتحكم في نظام محرك تيار مستمر . الهدف الرئيسي هو تحقيق تنظيم دقيق للسرعة وأداء قوي تحت ظروف تشغيل مختلفة، بما في ذلك تغير الحمل والاضطرابات الخارجية. يتم تطوير نموذج رياضي للمحرك اعتمادًا على الديناميكيات الكهربائية والميكانيكية. لتحسين أداء النظام، يتم تطبيق عدة استراتيجيات للتحكم والتقدير، مثل المتحكم التناسبي التكاملي (PI)، وتقنيات المراقب المتقدمة مثل مراقب الوضع المنزلق (SMO)، ومراقب ليوينبرغر، ومراقب الحالة الموسعة (ESO) ضمن إطار التحكم برفض الاضطرابات النشط (ADRC). تهدف هذه الطرق إلى تحسين رفض الاضطرابات، وزيادة دقة التتبع، وتقدير المتغيرات غير المقاسة مثل السرعة وعزم الحمل. تُظهر نتائج المحاكاة أن استخدام المراقبات يحسن بشكل كبير الاستجابة الديناميكية، ويقلل من الخطأ في الحالة المستقرة، ويزيد من متانة النظام مقارنةً بالتحكم التقليدي.

Acknowledgements

First and foremost, we would like to express our sincere gratitude to Allah for granting us the strength, patience, and determination to complete this work.

We would like to extend our deepest appreciation to our supervisors, Mr. BENDJEDIA Bachir and Mr. BOUGRINE Djameleddine, for their invaluable guidance, patience, continuous support, and encouragement throughout the preparation of this master's thesis. Their scientific expertise, constructive remarks, and constant availability contributed greatly to the development and successful completion of this work. Working under their supervision has been a highly enriching and rewarding experience, and we are truly grateful for the confidence and trust they placed in us during this research journey.

We also express our sincere thanks to all the teachers and staff members of the Faculty of Technology for the quality of education and support they provided throughout our academic studies. Their efforts played an essential role in building the knowledge and skills that enabled us to accomplish this thesis.

Our heartfelt appreciation also goes to our families for their unconditional love, patience, sacrifices, and continuous encouragement. Words cannot fully express how grateful we are to our parents for all the support they have given us throughout our studies. Their prayers, understanding and motivation have always been a source of strength and determination during difficult moments. We are equally grateful to our siblings and relatives for their encouragement and moral support throughout this journey.

Finally, we express our special thanks to the members of the LACoSERE Laboratory for their valuable discussions, collaboration, and friendly working environment. Their support and scientific exchanges greatly facilitated the realization of this work and contributed significantly to its completion.

LAGGOUN Safa Malak
NEKKAR Melissa
Laghouat University
June 2026

List of Abbreviations

Abbreviation	**Description**
ADRC	Active Disturbance Rejection Control
BLDC	Brushless DC Motor
DC	Direct Current
ECU	Electronic Control Unit
EKF	Extended Kalman Filter
ESO	Extended State Observer
EV	Electric Vehicle
FOC	Field-Oriented Control
H-Bridge	Full-Bridge Power Converter
IM	Induction Motor
NEDC	New European Driving Cycle
PI	Proportional–Integral Controller
PMSM	Permanent Magnet Synchronous Motor
PWM	Pulse Width Modulation
SMO	Sliding Mode Observer
ST-SMO	Super-Twisting Sliding Mode Observer
VSI	Voltage Source Inverter
i_a	Armature Current
L_a (or L)	Armature Inductance
R_a (or R)	Armature Resistance
e_b	Back Electromotive Force (Back EMF)
K_e	Back EMF Constant
K_t	Torque Constant
τ / T_e	Electromagnetic Torque
T_L	Load Torque
J	Moment of Inertia of the Rotor
B (or b)	Viscous Friction Coefficient
V_a	Armature Voltage

Abbreviation	**Description**
V_{ref}	Reference Voltage
V_{out}	Output Voltage
ω	Angular Speed (rad/s)
$\dot{\omega}$	Angular Acceleration

Contents

Abstract **2**

Acknowledgements **3**

List of Abbreviations **4**

Contents **6**

General Introduction **10**

1 Load Torque Disturbance Estimation and Compensation for High-Performance Electric Vehicle Motor Drives **12**

1.1 Introduction 12
1.2 EV Propulsion Architecture 13
1.3 Types of electric motors used in EVs (DC, IM, PMSM, BLDC) 14
1.3.1 Power Electronic Converters and Control Structure 15
1.3.2 Requirements for High-Performance EV Drives (Accuracy, Robustness, Efficiency) 16
1.4 Load Torque Estimation Techniques 16
1.4.1 Classical Estimation Methods 16
1.5 Literature Review 17
1.5.1 Study 1: Sliding Mode Observer-Based Load Torque Identification for PMSM Drives [1] 17
1.5.2 Study 2: A Review on Robust Predictive Control of Permanent Magnet Synchronous Motor Drives: Strategies and Future Trends [2] 18
1.5.3 Study 3: Motor Torque Estimation and Security Control for Electric Vehicles Based on Parameters Feature Extraction [3] 18
1.5.4 Study 4: Load Torque Observation and Compensation for Permanent Magnet Synchronous Motor Based on Sliding Mode Observer [4] 19
1.5.5 Observer-Based Approaches (Luenberger and Kalman Filter) 19
1.5.6 Comparative Analysis of Estimation Methods 21
1.6 Load Torque Compensation Strategies 21
1.6.1 Feedforward Compensation Techniques 21
1.6.2 Feedback-Based Compensation 22
1.6.3 Robust Control Approaches 22
1.7 Proposed Estimation and Compensation Scheme 22
1.7.1 Control System Architecture 22

1.7.2 Design of the Proposed Observer/Estimator 22
1.8 Proposed Methodology of the Thesis 23
1.9 Conclusion 24

2 Design and Analytical Development of Load Torque Observers with Open-Loop and Experimental Validation 25
2.1 Introduction 25
2.2 Modeling of the DC Motor 25
2.2.1 Physical Structure of the DC Motor 26
2.2.2 Mathematical Modeling 26
2.2.3 Electromechanical Coupling 27
2.2.4 State-Space Representation 27
2.2.5 Observability and Stability 28
2.3 Mathematical Formulas 29
2.3.1 Mathematical Formulation of Luenberger Observer 29
2.3.2 Mathematical Formulation Extended State Observer (ESO) (used in ADRC controller) 30
2.3.3 Gain Design of ESO 32
2.3.4 Mathematical Formulation of Sliding Mode Observer (SMO) . . . 33
2.3.5 Super-Twisting Sliding Mode Observer (ST-SMO) 35
2.4 Simulation Framework 36
2.5 Robustness Evaluation of Load Torque Observers Under Motor Parameter Variations 39
2.5.1 Sumilation Results 39
2.6 Experimental Validation of Luenberger Observer and Extended State Observer (ESO) 44
2.6.1 Experimental Test Bench Description 45
2.6.2 System Modeling and Observation Framework 46
2.6.3 Implementation of Luenberger Observer 46
2.6.4 Implementation of Extended State Observer (ESO) 46
2.6.5 Experimental Procedure 46
2.6.6 Results and Discussion 46
2.6.7 Performance Comparison 49
2.6.8 Conclusion of Experimental Validation 49
2.7 Conclusion 49

3 Motor Torque Estimation for Disturbance Compensation and Secure Speed Control in Electric Vehicle Applications 50
3.1 Introduction 50
3.2 Proposed Topology of the DC Drive 50
3.2.1 Battery Pack 51
3.2.2 H-Bridge Power Converter 51
3.2.3 DC Motor and Mechanical Transmission 51
3.2.4 PWM Generation Unit 52
3.2.5 DC Motor 52
3.2.6 Sensors 52
3.3 Control Scheme 53
3.3.1 Speed Control Loop 53

3.3.2 Current Control Loop 54
3.3.3 Controller Tuning 55
3.3.4 Observer Integration and Torque Estimation 55
3.4 Simulation Results 55
3.4.1 Simulation Without Torque Estimation 56
3.4.2 Simulation With Torque Estimation 56
3.5 Application to a Real Electric Vehicle Scenario 60
3.5.1 Dynamic Model of the Electric Vehicle 60
3.5.2 Driving Cycle 62
3.5.3 Torque and Speed Profiles 63
3.6 Discussion of Results 67
3.7 Conclusion 67

General Conclusion **69**

List of Figures

1.1 Electric Vehicle Propulsion Architecture 14
1.2 Feedforward Compensation Techniques 21
1.3 Feedback-Based Compensation 22

2.1 Electromechanical Equivalent Circuit of a DC Motor 26
2.2 Luenberger Observe MATLAB design 29
2.3 ESO MATLAB design 33
2.4 Sliding Mode MATLAB design 34
2.5 Sliding Mode Extreme MATLAB design 35
2.6 Tracking Torque Load in open-loop 38
2.7 Torque Error 38
2.8 Simulink Analysis of R Parameter Variation 39
2.9 Simulink Analysis of L Parameter Variation 41
2.10 Simulink Analysis of K Parameter Variation 42
2.11 Simulink Analysis of F Parameter Variation 43
2.12 Simulink Analysis of J Parameter Variation 44
2.13 Overall Topology 45
2.14 EXPERIMENTAL RESULTS : SPEED 47
2.15 EXPERIMENTAL RESULTS : CURRENT 47
2.16 EXPERIMENTAL RESULTS : ESTIMATED TORQUES 48
2.17 EXPERIMENTAL RESULTS : ESTIMATED ERRORS 48

3.1 Overall topology of the proposed DC motor drive system. 51
3.2 Block diagram of the proposed cascaded speed and current control scheme with observer-based with torque estimation. 53
3.3 Speed responses 57
3.4 Estimation error responses 57
3.5 Current responses 58
3.6 Torque estimation responses 59
3.7 Simplified urban driving cycle used as speed reference for the EV simulation. 60
3.8 URBAN PART OF NEDC DRIVING SYCLE 63
3.9 Reference speed profile for 1 kW DC motor drive 64
3.10 Load torque profile for 1 kW DC motor drive 64
3.11 Power profile for 1 kW DC motor drive 65
3.12 Speed Response During the Electric Vehicle Driving Cycle. 65
3.13 Loude Torque Response of ESO-ADRC ,SMO1 ,SMO2 ,Luenberger. 66
3.14 Motor Power Response During the Electric Vehicle Driving Cycle. 66

General Introduction

The transportation sector is currently undergoing a profound transformation driven by the increasing demand for sustainable mobility solutions, the depletion of fossil fuel resources, and the need to reduce greenhouse gas emissions. In this context, Electric Vehicles (EVs) have emerged as a promising alternative to conventional internal combustion engine vehicles due to their high energy efficiency, low environmental impact, reduced maintenance requirements, and superior dynamic performance.

The performance of an electric vehicle largely depends on the efficiency and control of its electric propulsion system. Electric motors offer several advantages over conventional engines, including high torque density, fast dynamic response, and the capability to operate in both motoring and regenerative braking modes. These characteristics make electric drives particularly suitable for transportation applications where precise speed and torque regulation are essential.

Among the various challenges encountered in electric drive systems, the presence of load torque disturbances represents a major factor affecting control performance. In electric vehicle applications, load torque variations arise from changes in road conditions, vehicle mass, rolling resistance, aerodynamic drag, and external disturbances. These factors introduce uncertainties that can degrade speed regulation, increase tracking errors, and reduce the overall robustness of the propulsion system.

To ensure high-performance operation under such conditions, advanced control and estimation techniques have become indispensable. In particular, observer-based approaches provide an effective solution for estimating unknown variables and disturbances that cannot be measured directly. By accurately reconstructing the load torque, these methods enable the controller to compensate for external perturbations and maintain the desired dynamic performance.

The present work focuses on the design, analysis, and application of load torque observers for electric motor drive systems intended for electric vehicle propulsion. Several estimation techniques are investigated, including the Luenberger Observer, Sliding Mode Observer, and Extended State Observer based on the Active Disturbance Rejection Control (ADRC) framework. Their mathematical formulation and estimation principles are studied to evaluate their ability to reconstruct load torque disturbances under various operating conditions.

Following the observer design stage, the proposed estimation methods are integrated into a complete closed-loop DC motor drive system incorporating current and speed control loops. Extensive simulations are conducted to assess the influence of load torque estimation on the dynamic behavior of the drive system. Comparative analyses are performed

to evaluate the effectiveness of each observer in terms of estimation accuracy, disturbance rejection capability, speed tracking performance, and robustness.

Finally, the developed methodology is applied to a reduced-scale electric vehicle propulsion system driven by a 1.5 kW DC motor. A dynamic vehicle model is considered to reproduce realistic driving conditions, allowing the assessment of the proposed observer-based control strategy in practical electric mobility applications.

This thesis is organized as follows:

- Chapter 1 presents the fundamentals of electric vehicle propulsion systems, the importance of torque control, and a review of load torque estimation techniques reported in the literature.
- Chapter 2 develops the mathematical formulation and design of the proposed load torque observers, including the Luenberger Observer, Sliding Mode Observer, and Extended State Observer. Their estimation performances are evaluated under open-loop operating conditions.
- Chapter 3 focuses on the implementation of the proposed load torque observers within a closed-loop DC motor drive system and their application to an electric vehicle propulsion system. Comparative simulations are performed under various operating conditions and driving scenarios to evaluate estimation accuracy, disturbance rejection capability, and speed control performance.
- Finally, the thesis concludes with a summary of the main contributions and outlines future research directions.

Chapter 1

Load Torque Disturbance Estimation and Compensation for High-Performance Electric Vehicle Motor Drives

---

1.1 Introduction

An Electric Vehicle (EV) is a transportation system propelled by one or more electric motors, which replace the conventional internal combustion engine for propulsion. In EV architectures, electrical energy stored in the battery is converted into mechanical motion through an electric traction drive system.

Compared with conventional vehicles, EVs offer several advantages, including higher energy efficiency, reduced emissions, lower maintenance requirements, quieter operation, and superior dynamic performance. One of the most significant characteristics of electric machines is their ability to deliver maximum torque almost instantaneously, which enables excellent acceleration and highly responsive dynamic behavior.

Modern EV propulsion systems are highly integrated and typically consist of an electrochemical energy storage system (battery pack), power electronic converters (inverters), electric machines, and mechanical transmission elements. Among these components, the electric motor—most commonly a Permanent Magnet Synchronous Motor (PMSM) or an Induction Motor (IM)—acts as the main actuator responsible for converting electrical energy into mechanical tractive force.

Unlike internal combustion engines, electric machines provide high power density, wide operating-range efficiency, fast torque response, and bidirectional energy capability enabling regenerative braking. However, fully exploiting these advantages requires advanced control strategies capable of ensuring precise torque regulation, fast dynamic response, and robust operation under varying driving conditions, road profiles, and external disturbances.

In this context, torque control plays a central role in achieving high-performance operation of electric motor drives. Accurate torque regulation is essential to ensure smooth

vehicle dynamics, precise speed tracking, reduced torque ripple, and improved drivability. Nevertheless, the performance of torque-controlled systems is significantly affected by load torque disturbances, which arise from road slope variations, vehicle mass changes, rolling resistance, aerodynamic effects, and mechanical uncertainties. These disturbances are generally unknown and time-varying, and they introduce performance degradation in terms of speed deviation, tracking errors, and reduced robustness.

To overcome these limitations, a wide range of load torque estimation techniques has been developed in the literature, including classical model-based methods, observer-based approaches such as Luenberger and Kalman filters, adaptive techniques such as MRAS, robust methods such as sliding mode observers, and more recent intelligent approaches based on artificial intelligence.

Accordingly, this chapter presents a comprehensive study of high-performance torque control in electric vehicle motor drives. It first highlights the importance of torque control in modern EV applications, then discusses the impact of load torque disturbances on system performance degradation, and finally reviews the main methods used for load torque estimation. This study provides the necessary background for the development of advanced estimation and compensation strategies presented in the subsequent sections of this work.

1.2 EV Propulsion Architecture

The electric vehicle (EV) propulsion architecture is a highly integrated electromechanical system designed to convert electrical energy stored in the battery into controlled mechanical traction at the wheels. A typical EV propulsion system is composed of several interconnected subsystems, each playing a specific role in energy conversion, control, and power delivery.

The main components of a standard EV propulsion architecture include:

- **Energy Storage System:** The battery pack (typically lithium-ion) serves as the primary energy source. It supplies the DC electrical power required by the propulsion system and auxiliary loads.
- **Power Electronic Converter:** The inverter converts DC voltage from the battery into a controlled three-phase AC supply for the electric motor. It also enables bidirectional power flow, which is essential for regenerative braking operation.
- **Electric Motor:** The traction motor, commonly a Permanent Magnet Synchronous Motor (PMSM) or an Induction Motor (IM), converts electrical energy into mechanical torque. It represents the core actuator of the propulsion system.
- **Transmission System:** A mechanical gearbox or single-speed reduction gear transmits the motor torque to the wheels while adapting speed and torque levels to driving requirements.
- **Control Unit:** The electronic control unit (ECU) implements advanced control algorithms such as Field-Oriented Control (FOC), ensuring precise regulation of torque, speed, and flux. It also coordinates energy management and system protection.

In this architecture, energy flows from the battery through the inverter to the electric motor, which generates mechanical torque transmitted to the wheels. During regenerative braking, this energy flow is reversed, allowing the motor to operate as a generator and recover kinetic energy back to the battery.

This tightly coupled architecture requires high-performance control strategies to ensure efficient energy conversion, fast dynamic response, and robust operation under varying driving conditions and load disturbances.

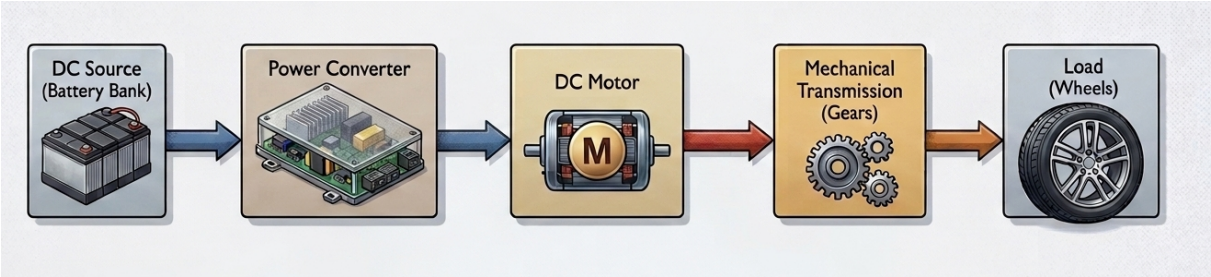


Figure 1.1: Electric Vehicle Propulsion Architecture

1.3 Types of electric motors used in EVs (DC, IM, PMSM, BLDC)

The electric motor serves as the primary electromechanical actuator responsible for converting electrical energy into mechanical traction torque. Selecting an appropriate motor architecture involves balancing structural simplicity, power density, thermal resilience, and control complexity.

Direct Current (DC) Motor Drives

The Direct Current (DC) motor is a cost-effective electromechanical actuator known for its straightforward design, easily regulated speed, and high starting torque. However, its reliance on a physical brush and commutator assembly introduces significant mechanical drawbacks, including continuous friction wear, electrical sparking, and inherently lower operational efficiencies. These structural limitations restrict high-speed performance and necessitate regular maintenance, confining the contemporary use of DC motors primarily to low-power and educational traction applications.

Brushless DC Motor

The Brushless DC Motor advances traditional motor design by replacing mechanical brushes with solid-state electronic commutation. Utilizing rotor-mounted permanent magnets and electronically sequenced stator windings, this architecture delivers superior operational efficiency, high power density, minimal maintenance, and a robust dynamic response. However, these advantages are offset by the need for complex control algorithms, higher multi-phase inverter manufacturing costs, and potential torque ripple at low speeds. Despite these control complexities, their optimized performance-to-volume ratio makes DC motors the prevalent choice for light electromobility applications, including micro-EVs, drones, and electric bicycles.

Permanent Magnet Synchronous Motor (PMSM)

The Permanent Magnet Synchronous Motor (PMSM) is one of the most widely used propulsion technologies in electric vehicles due to its high efficiency, high power density, fast torque response, compact design, and low noise operation. Its rotor contains permanent magnets, while the stator generates a rotating magnetic field to produce electromagnetic torque through vector-controlled (d)-(q) axis current regulation. These advantages make PMSMs the preferred choice for passenger EVs, high-performance electric vehicles, and autonomous driving platforms. However, their dependence on expensive rare-earth magnets increases manufacturing costs, and the rotor is vulnerable to thermal demagnetization at high temperatures. In addition, achieving optimal performance requires sophisticated control techniques such as Field-Oriented Control (FOC), increasing system complexity despite the motor's superior performance characteristics.

Induction Motor (IM)

The Induction Motor (IM) is a robust electric vehicle propulsion technology that operates without rare-earth permanent magnets, generating rotor currents through electromagnetic induction. Its key advantages include low manufacturing cost, high reliability, minimal maintenance requirements, strong fault tolerance, and excellent performance in high-speed field-weakening operation, making it well suited for commercial EVs, electric buses, and heavy-duty traction applications. However, compared to PMSMs, induction motors exhibit lower efficiency, require a larger physical size, and generate greater heat losses due to slip and inductive excitation. Despite these limitations, their durability, cost-effectiveness, and reliability make them a popular choice for high-power electric transportation systems.

1.3.1 Power Electronic Converters and Control Structure

Power electronic converters are essential components in electric vehicle (EV) propulsion systems, as they interface the DC energy source (battery) with the AC electric motor. Their main role is to regulate the energy flow, control motor operating conditions, and ensure efficient and reliable power conversion under dynamic driving conditions.

In most EV applications, the voltage source inverter (VSI) is the dominant topology used to supply three-phase AC voltages to the motor. The inverter operates through high-frequency switching devices such as IGBTs or MOSFETs, enabling precise control of voltage magnitude and frequency. This allows continuous adjustment of motor torque and speed according to driver demand and road conditions.

The control structure of EV drives is typically based on a hierarchical architecture. At the inner level, fast current control loops regulate the motor phase currents to directly control electromagnetic torque and flux. At the outer level, speed or torque control loops generate reference currents based on driving requirements. Field-Oriented Control (FOC) is widely adopted, as it decouples torque and flux components, enabling high dynamic performance similar to DC motor control behavior.

Advanced modulation techniques such as Pulse Width Modulation (PWM) or Space Vector PWM (SVPWM) are commonly used to optimize switching performance, reduce harmonic distortion, and improve overall efficiency of the drive system.

1.3.2 Requirements for High-Performance EV Drives (Accuracy, Robustness, Efficiency)

High-performance electric vehicle drives must satisfy stringent requirements to ensure safe, efficient, and comfortable operation under all driving conditions. These requirements can be summarized in terms of accuracy, robustness, and efficiency.

Accuracy refers to the ability of the drive system to precisely track reference speed and torque commands. High tracking accuracy is essential to ensure smooth vehicle behavior, rapid response to driver inputs, and minimal steady-state error, particularly during transient conditions such as acceleration and deceleration.

Robustness is the capability of the drive system to maintain satisfactory performance despite uncertainties, disturbances, and parameter variations. In EV applications, these include load torque disturbances, battery voltage fluctuations, temperature effects, and variations in motor parameters. A robust control system ensures stability and performance even under harsh and unpredictable operating conditions.

Efficiency is a critical requirement in EV systems, as it directly impacts driving range and energy consumption. High efficiency must be achieved across a wide operating range, including low-speed, high-torque, and high-speed operating regions. This involves minimizing power losses in the inverter, motor, and mechanical transmission while optimizing energy utilization through techniques such as regenerative braking and optimal control strategies.

1.4 Load Torque Estimation Techniques

Accurate estimation of load torque is a key requirement for achieving high-performance control in electric motor drives, particularly in electric vehicle (EV) applications. Since load torque cannot be directly measured in most practical systems, it must be reconstructed using mathematical models, observers, or intelligent estimation strategies. Over the years, several estimation techniques have been proposed, ranging from classical analytical approaches to advanced observer-based and data-driven methods.

1.4.1 Classical Estimation Methods

Classical load torque estimation methods are primarily based on the mechanical dynamics of the motor drive system. By rearranging the equation of motion, the load torque can be estimated using measurable quantities such as electromagnetic torque, angular speed, and angular acceleration. These approaches rely on the following mechanical model:

$$T_L = T_e - J\frac{d\omega}{dt} - B\omega \tag{1.1}$$

Although conceptually simple, classical methods suffer from significant drawbacks in practical applications. The differentiation of speed signals amplifies measurement noise, and the accuracy of the estimation strongly depends on precise knowledge of system parameters such as inertia J and friction coefficient B. Consequently, their performance deteriorates under parameter uncertainties and noisy environments, which are typical in EV systems.

1.5 Literature Review

The literature review provides an overview of the main research efforts related to electric motor drive systems, with particular emphasis on disturbance estimation and robust control strategies. Numerous studies have investigated the effects of load torque disturbances, parameter uncertainties, and external perturbations on drive performance. To address these challenges, various estimation and compensation techniques have been proposed, including Luenberger observers, disturbance observers, Kalman filters, sliding-mode observers, and adaptive estimation methods. This review aims to analyze the strengths and limitations of existing approaches, identify current research trends, and highlight the remaining challenges in load torque estimation for high-performance motor drive applications such as electric vehicles, robotics, and industrial automation. The relevant studies are summarized in Table 2.4

1.5.1 Study 1: Sliding Mode Observer-Based Load Torque Identification for PMSM Drives [1]

(Master's Thesis, Aalborg University)

This research addresses the speed control optimization of a surface-mounted permanent magnet synchronous motor (SPMSM). To alleviate speed performance degradation under time-varying load torque disturbances, the authors introduce an online load torque estimation technique utilizing four distinct Sliding Mode Observer (SMO) configurations. The dynamically estimated torque is mapped directly as a feed-forward compensation term to suppress speed tracking deviations, thereby reducing recovery times and enhancing the transient response of traditional proportional-integral (PI) controllers.

Advantages and Advancements: In terms of architectural advancements, this study successfully minimizes the chattering phenomenon inherent to conventional sliding mode frameworks by implementing a modified Sigmoid function as a continuous switching boundary condition. This design effectively suppresses high-frequency oscillations and eliminates the necessity for an auxiliary low-pass filter (LPF), thereby averting detrimental phase delays within the feedback loop. Furthermore, the proposed schemes undergo a comprehensive verification process by contrasting four distinct observer iterations through detailed Matlab/Simulink simulations and physical experimental test bench validation.

Limitations and Weaknesses: Conversely, a critical vulnerability of this methodology lies in its high sensitivity to physical measurement noise. Because the underlying SMO models rely heavily on measured mechanical speed as a primary state input, baseline mechanical frequencies or speed ripples present even during un-loaded states are falsely interpreted by the observer as external load variations. This structural error subsequently amplifies high-frequency sub-harmonics during physical implementation, effectively doubling the amplitude of sub-harmonic ripples within the 35 Hz to 40 Hz band due to calculation errors stemming from current (i_q) and speed feedback loops.

1.5.2 Study 2: A Review on Robust Predictive Control of Permanent Magnet Synchronous Motor Drives: Strategies and Future Trends [2]

(Review Article, AIP Advances)

This comprehensive review classifies and analyzes robust predictive control strategies developed to mitigate model uncertainties (such as internal inductance or flux linkages mismatches) and non-model variations (including cogging torque, torsional vibration, backlash, and external disturbances) within modern motor drive topologies.

Advantages and Advancements: The core merit of this work lies in its systematic categorization and high-level synthesis of modern control paradigms. It evaluates the operational strengths of modern Disturbance Observers (such as Extended State Observers and standard SMOs), online Parameter Identification techniques (such as high-frequency signal injection), and Predictive Model improvements. Additionally, it offers valuable projections regarding future control architectures, focusing on multi-vector predictive control to limit inverter switching frequencies and artificial intelligence data-driven strategies that completely bypass physical parameter modeling.

Limitations and Weaknesses: However, the literature highlights severe structural and computational trade-offs embedded within these state-of-the-art architectures. Online parameter identification paradigms inherently demand immense real-time computing power and weaken immediate anti-disturbance tracking capabilities, whereas traditional disturbance observers require overly complex mathematical layouts. Furthermore, as a review article, the study lacks original empirical validation, failing to provide new physical experimental test data or a single, unified benchmark architecture under uniform testing criteria.

1.5.3 Study 3: Motor Torque Estimation and Security Control for Electric Vehicles Based on Parameters Feature Extraction [3]

(Research Article, Advances in Mechanical Engineering)

This study develops a powertrain security framework aimed at mitigating functional safety risks, such as unpredictable electric vehicle (EV) acceleration or deceleration, induced by stochastic hardware or software controller faults. The methodology extracts three-phase voltage and current feature parameters to calculate real-time motor torque online. It introduces a Quality Factor (QF) alongside confidence coefficients to identify abnormal calculation trends and instantly restrains faulty torque propagation by executing software-level fault flags.

Advantages and Advancements: This methodology significantly contributes to the domain of functional safety by aligning powertrain monitoring with ISO 26262 objectives, enabling the Motor Control Unit (MCU) to shift seamlessly into an active secure state upon detecting a torque envelope violation. The layout implements strict plausibility checking through rigorous data filtering and confidence-flag validation loops on voltage

and current inputs, safeguarding the calculation module against sensor noise errors. Physical test bench validation demonstrated high tracking accuracy, restricting the estimation error to a tight ±5 Nm envelope relative to actual physical sensor measurements.

Limitations and Weaknesses: Nonetheless, the system is constrained by a highly complex control layer dependency. By relying exclusively on multi-variable three-phase input features, simultaneous sensor or phase-fault breakdowns can distort the confidence metrics and disrupt the security mapping logic. Additionally, the scope of the dynamic transient evaluation is limited, as the research primarily focuses on executing discrete binary fault-flag isolation rather than demonstrating smooth, continuous speed regulation and recovery under fast-changing dynamic load profiles during non-fault operations.

1.5.4 Study 4: Load Torque Observation and Compensation for Permanent Magnet Synchronous Motor Based on Sliding Mode Observer [4]

(Research Article, Cobot)

The authors present a finite-time sliding mode observer designed to track time-varying load disturbances on a PMSM, converting the observed disturbance into a q-axis feed-forward compensation current to dampen speed fluctuations. A Genetic Algorithm (GA) is utilized to automatically optimize the observer gains by minimizing the Integral of Time-weighted Absolute Error (ITAE) index.

Advantages and Advancements: The practical efficacy of this strategy is evidenced by a substantial reduction in speed deviations. Experimental evaluations performed on a dedicated torque platform demonstrated that integrating the feed-forward compensation loop reduces overall motor speed fluctuations by approximately 60% during sudden load variations. Additionally, the integration of a Genetic Algorithm effectively automates parameter tuning, bypassing tedious manual trial-and-error procedures for setting the observer constants (g and k) to achieve an optimal balance between dynamic responsiveness and jitter reduction.

Limitations and Weaknesses: Despite these benefits, the study possesses notable standardization and validation deficiencies. The paper was published as a Version 1 subject to substantial peer-review reservations, with evaluators noting that several primary conclusions were unsupported by the provided data. A key limitation is the incomplete transient assessment, as the study explicitly omits data or analysis concerning transient speed performance during sudden load decreases (unloading behavior). Furthermore, minor mathematical formulations within the introductory sections lack standardization, such as the non-standard designation of the i_α current vector.

1.5.5 Observer-Based Approaches (Luenberger and Kalman Filter)

Otherwise, observer-based methods improve estimation accuracy by reconstructing unmeasured states of the system using dynamic models and feedback correction.

Table 1.1: Comparison of Observer-Based Studies

Study	**Observer / Estimator Used**	**Strengths**	**Weaknesses**
Wang et al. (2025) *A Review on Robust Predictive Control of PMSM Drives*	Reviews multiple observers including: • Extended State Observer (ESO) • Sliding Mode Observer (SMO) • Kalman Filter • Adaptive Observers	• Comprehensive overview of robust PMSM control methods • Covers disturbance rejection and parameter uncertainty compensation • Useful reference for selecting observer structures	• No new observer proposed • No experimental validation • Limited discussion of implementation complexity
Lu et al. (2024) *Load Torque Observation and Compensation for PMSM Based on Sliding Mode Observer*	Sliding Mode Observer (SMO) optimized using a Genetic Algorithm (GA)	• Robust against disturbances and model uncertainties • No additional torque sensor required • Feedforward compensation reduces speed fluctuation by approximately 60% • Experimentally validated	• Chattering inherent to classical SMO • Tested under limited operating conditions • Observer performance depends on parameter accuracy
Aalborg University Thesis (2022) *Sliding Mode Observer-Based Load Torque Identification for PMSM Drives*	Four observer variants: • Sign-function SMO • Saturation-function SMO • Power-Sigmoid + PI SMO	• Comprehensive comparison of multiple SMO structures • Experimental and simulation validation • Lyapunov-based stability analysis • Saturation observers significantly reduce speed error and recovery time	• Assumes ideal PMSM conditions • Limited speed/load test conditions • Observer tuning remains complex • Sensitive to modelling inaccuracies

The Luenberger observer is one of the earliest state estimation techniques, where the system is augmented to include load torque as an additional state variable. The observer estimates the system states by minimizing the error between measured and estimated outputs. However, its performance is sensitive to modeling inaccuracies and is mainly suitable for linear or mildly nonlinear systems.

The Kalman filter and its extended version (EKF) provide an optimal estimation framework in the presence of noise. By considering statistical models of process and measurement noise, the Kalman filter achieves improved robustness and accuracy. Nevertheless, its effectiveness depends heavily on accurate tuning of covariance matrices, which can be challenging in real EV operating conditions.

1.5.6 Comparative Analysis of Estimation Methods

Different load torque estimation techniques exhibit distinct advantages and limitations. Classical methods are simple and easy to implement but are highly sensitive to noise and parameter variations. Observer-based approaches, such as Luenberger observers, offer improved performance but are limited by model accuracy and system linearity assumptions. Kalman filter-based methods provide optimal estimation in stochastic environments but require precise noise modeling and increased computational effort. In summary, there is a clear trade-off between simplicity, robustness, and computational complexity among the different estimation methods. This motivates the development of more advanced and robust estimation strategies capable of ensuring reliable performance under the highly variable operating conditions of electric vehicle systems.

1.6 Load Torque Compensation Strategies

Load torque compensation strategies are designed to mitigate the adverse effects of external disturbances on electric motor drive performance. Once the load torque is estimated, it can be actively compensated within the control loop to improve speed regulation, torque tracking, and overall system robustness.

1.6.1 Feedforward Compensation Techniques

Feedforward compensation is one of the most widely used strategies in which the estimated load torque is directly injected into the control law. By anticipating the disturbance effect, the controller can counteract its influence before it propagates through the system dynamics. This approach is simple and effective, provided that the estimation accuracy is sufficiently high. Look Figure 1.2.

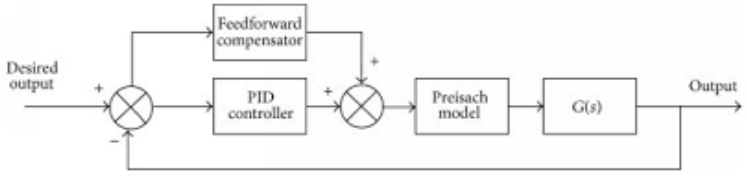


Figure 1.2: Feedforward Compensation Techniques

1.6.2 Feedback-Based Compensation

In feedback-based compensation, the estimated load torque is integrated into the closed-loop control system. The controller continuously adjusts the control input based on the error between reference and measured variables, while also considering the estimated disturbance. This improves disturbance rejection capability and enhances steady-state performance. as showen in figure 1.3.

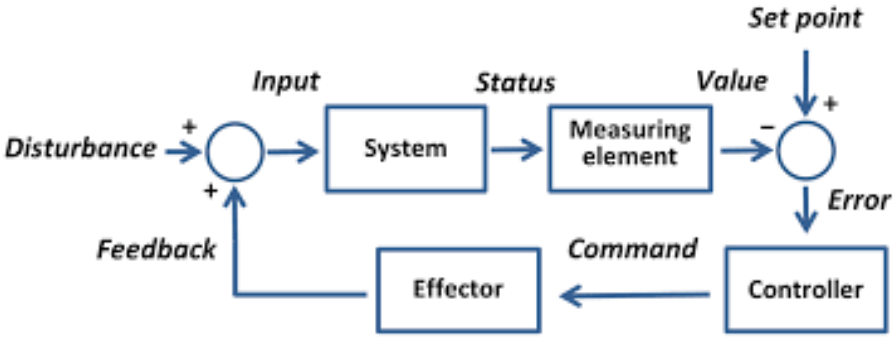


Figure 1.3: Feedback-Based Compensation

1.6.3 Robust Control Approaches

Robust control techniques such as sliding mode control and adaptive control are frequently employed to handle uncertainties and disturbances in load torque. These methods ensure system stability under parameter variations and external perturbations. However, they may introduce challenges such as chattering or increased controller complexity.

1.7 Proposed Estimation and Compensation Scheme

1.7.1 Control System Architecture

The proposed control scheme integrates a load torque estimation mechanism within a field-oriented control (FOC) structure for electric vehicle motor drives. The architecture consists of an outer speed control loop, inner current control loops, and a disturbance estimation block. The estimated load torque is fed back into the control system to improve torque regulation and dynamic response under varying operating conditions.

1.7.2 Design of the Proposed Observer/Estimator

The proposed observer is designed to estimate the load torque in real time based on the motor's mechanical dynamics and measurable variables such as rotor speed and electromagnetic torque. The estimation model augments the state-space representation of the system by including load torque as an additional state variable.

The observer gain is selected to ensure fast convergence of the estimation error while maintaining robustness against noise and parameter uncertainties. The estimated load torque is then used in a compensation law to cancel the effect of external disturbances and improve system performance. This integrated approach enhances both transient and steady-state behavior of the electric drive system.

1.8 Proposed Methodology of the Thesis

Modern electric vehicles (EVs) predominantly employ high-performance traction machines such as Permanent Magnet Synchronous Motors (PMSMs), Brushless DC Motors (BLDCs), and Induction Motors (IMs), owing to their superior efficiency, high power density, and excellent dynamic response characteristics. Among these technologies, PMSMs and BLDC motors have become particularly prominent in automotive applications due to their high torque-to-inertia ratio, wide constant-power speed range, and overall suitability for electrified propulsion systems. Nevertheless, these advantages come at the cost of increased system complexity, requiring advanced control strategies and accurate mathematical modeling to fully exploit their performance potential.

In this work, a DC motor is adopted as the traction machine. This choice is justified by its well-established and analytically tractable mathematical model, its inherently decoupled speed and torque characteristics, and its ease of implementation in both simulation and experimental platforms. As such, it provides a suitable and robust testbed for the development, validation, and performance assessment of electric traction control and disturbance estimation strategies.

Furthermore, a single-motor electric vehicle architecture is considered in order to reduce system complexity while preserving the essential dynamic behavior of EV propulsion systems. This configuration is widely adopted in foundational studies and laboratory-scale implementations, as it enables a clear and direct analysis of the interaction between electromagnetic torque generation, load torque disturbances, and vehicle dynamic response.

For experimental validation, key system variables—including motor speed, armature current, and supply voltage—are acquired through appropriate sensing devices. These measurements constitute the basis for system identification, modeling, and performance evaluation under various operating conditions and disturbance scenarios. The complete methodology for estimation, control design, and performance analysis based on these measurements is developed and discussed in detail in Chapters 2 and 3, providing a structured framework for the proposed investigation.

1.9 Conclusion

This chapter has provided a comprehensive overview of load torque disturbance estimation and compensation in high-performance electric vehicle (EV) motor drives. The fundamental structure of EV propulsion systems was first presented, highlighting the key role of electric machines, power electronic converters, and control systems in achieving efficient and reliable traction performance.

A detailed classification of traction motor technologies, including DC motors, induction motors, PMSMs, and BLDC machines, was discussed, emphasizing their respective advantages and control requirements in modern EV applications. Particular attention was given to the importance of high-performance drive requirements, namely accuracy, robustness, and efficiency, which constitute essential performance criteria in automotive control systems.

The chapter further examined the origin and impact of load torque disturbances, which represent one of the most critical sources of performance degradation in electric drives. These disturbances, arising from road conditions, mechanical uncertainties, and external perturbations, directly affect speed regulation, torque tracking, and system stability.

In addition, a detailed review of load torque estimation techniques was presented, covering classical methods, observer-based approaches such as Luenberger and Kalman filters, sliding mode observers, and recent intelligent and adaptive strategies. A comparative analysis highlighted the trade-offs between simplicity, robustness, and computational complexity across the different methods.

Finally, load torque compensation strategies, including feedforward, feedback-based, and robust control approaches, were discussed, leading to the formulation of a general estimation and compensation framework.

Overall, this chapter establishes the theoretical and methodological foundation for the proposed research. It sets the basis for the development of advanced estimation and compensation strategies.

The second chapter will build directly on this foundation by presenting and developing different observer-based techniques for load torque estimation. These observers will be analyzed in terms of robustness and performance, and their effectiveness will be validated through MATLAB/Simulink simulations as well as experimental implementation, providing a comprehensive evaluation under realistic operating conditions.

Chapter 2

Design and Analytical Development of Load Torque Observers with Open-Loop and Experimental Validation

---

2.1 Introduction

This chapter presents the design and mathematical development of the proposed load torque observers, with a particular focus on their theoretical formulation and estimation principles. The mathematical models are derived to define the observer structures and to explain how unknown variables—especially external disturbances and load torque—can be accurately estimated from measurable system states.

The study encompasses both linear and nonlinear estimation strategies, including Luenberger observers, Sliding Mode Observers, and Extended State Observers (ESO) within the Active Disturbance Rejection Control (ADRC) framework. These approaches are developed in a unified analytical framework in order to highlight their respective design principles and estimation capabilities.

Following the mathematical formulation, the observers are first evaluated under open-loop conditions. This preliminary analysis allows the assessment of their intrinsic estimation performance without the influence of feedback correction. In particular, it provides insight into transient response, convergence behavior, estimation accuracy, and robustness limitations.

This step serves as a foundational validation stage before proceeding to closed-loop implementation, where the observers will be integrated into control schemes to enhance disturbance rejection and overall system performance.

2.2 Modeling of the DC Motor

The armature-controlled DC motor is one of the most widely used electromechanical systems in control engineering due to its simplicity, reliability, and ease of control. It is commonly used in robotics, electric vehicles, and industrial automation.

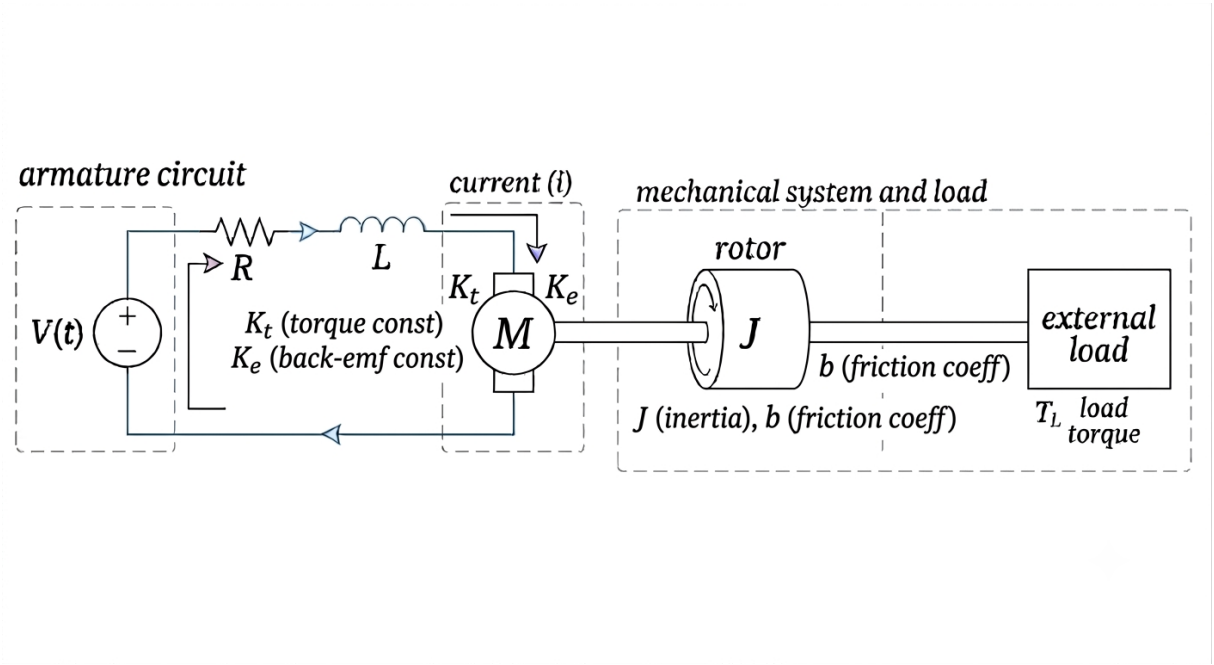


Figure 2.1: Electromechanical Equivalent Circuit of a DC Motor

2.2.1 Physical Structure of the DC Motor

A DC motor converts electrical energy into mechanical motion. Its operation involves two main subsystems:

- The electrical subsystem (armature circuit)
- The mechanical subsystem (rotor dynamics)

These subsystems are coupled through electromagnetic interactions, enabling energy conversion.

2.2.2 Mathematical Modeling

The dynamic behavior of the DC motor is described using:

- Newton's second law (mechanical dynamics)
- Kirchhoff's voltage law (electrical dynamics)

Mechanical Equation

The mechanical dynamics are given by:

$$J\dot{\omega} = -b\omega + K_t i - T_L \tag{2.1}$$

where:

- J is the moment of inertia
- b is the viscous friction coefficient

- ω is the angular speed
- K_t is the torque constant
- i is the armature current
- T_L is the load torque

The electromagnetic torque $K_t i$ drives the motor, while friction and load torque oppose motion. The load torque T_L represents an external disturbance acting on the motor. It is often unknown and affects the system performance by reducing the motor speed.

Electrical Equation

The electrical dynamics are described by:

$$L\dot{i} = -Ri - K_e\omega + u \tag{2.2}$$

where:

- L is the inductance
- R is the resistance
- K_e is the back-EMF constant
- u is the input voltage

The back-EMF term $K_e\omega$ represents the voltage generated by the motor rotation.

2.2.3 Electromechanical Coupling

The DC motor exhibits strong coupling between electrical and mechanical dynamics:

- Current i produces torque $K_t i$
- Speed ω produces back-EMF $K_e\omega$

In SI units, for an ideal motor:

$$K_t = K_e \tag{2.3}$$

2.2.4 State-Space Representation

Define the state vector:

$$x = \begin{bmatrix} \omega \\ i \end{bmatrix} \tag{2.4}$$

The system equations become:

$$\dot{\omega} = -\frac{b}{J}\omega + \frac{K_t}{J}i - \frac{1}{J}T_L \tag{2.5}$$

$$\dot{i} = -\frac{K_e}{L}\omega - \frac{R}{L}i + \frac{1}{L}u \tag{2.6}$$

Matrix Form

The system can be written as:

$$\dot{x} = Ax + Bu + ET_L \tag{2.7}$$

where:

$$A = \begin{bmatrix} -\frac{b}{J} & \frac{K_t}{J} \\ -\frac{K_e}{L} & -\frac{R}{L} \end{bmatrix}, \quad B = \begin{bmatrix} 0 \\ \frac{1}{L} \end{bmatrix}, \quad E = \begin{bmatrix} -\frac{1}{J} \\ 0 \end{bmatrix} \tag{2.8}$$

This uncertainty motivates the use of estimation techniques to reconstruct the disturbance.

2.2.5 Observability and Stability

For accurate estimation, the system must be observable:

$$\mathcal{O} = \begin{bmatrix} C \\ CA \\ CA^2 \\ \vdots \\ CA^{n-1} \end{bmatrix} \tag{2.9}$$

If:

$$\text{rank}(\mathcal{O}) = n \tag{2.10}$$

then the states can be reconstructed.

The estimation error is:

$$e(t) = x(t) - \hat{x}(t) \tag{2.11}$$

with dynamics:

$$\dot{e}(t) = (A - LC)e(t) + ET_L \tag{2.12}$$

If the eigenvalues of $(A - LC)$ have negative real parts, the observer is stable and the estimation error converges.

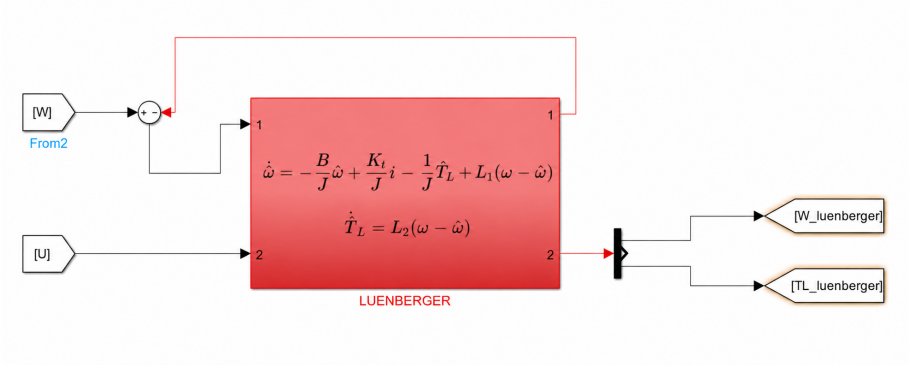


Figure 2.2: Luenberger Observe MATLAB design

2.3 Mathematical Formulas

2.3.1 Mathematical Formulation of Luenberger Observer

A Luenberger Observer is a state estimation method in control systems that reconstructs unmeasured system states using a mathematical model and measured outputs; it continuously corrects its estimate using feedback so the estimated states converge to the real system states over time.

Luenberger Observer

The observer is defined as:

$$\dot{\hat{x}}(t) = A\hat{x}(t) + Bu(t) + L(y - \hat{y}) \tag{2.13}$$

$$\hat{y}(t) = C\hat{x}(t) \tag{2.14}$$

The state-space matrices of the DC motor were obtained from the system parameters. The state matrix A and input matrix B are given as:

$$A = \begin{bmatrix} -117.9310 & -41.3793 \\ 300.0000 & -2.0000 \end{bmatrix}$$

$$B = \begin{bmatrix} 34.4828 \\ 0 \end{bmatrix}$$

In a Luenberger Observer, $\hat{x}(t)$ is the estimated state and (L) is the gain matrix, which is usually designed using pole placement to assign desired observer dynamics so the estimation error converges quickly and stably.(computed using pole placement), is:

$$L = \begin{bmatrix} -29.6468 \\ 580.0690 \\ -271.3450 \end{bmatrix}$$

These matrices were used for system modeling and state estimation.

2.3.2 Mathematical Formulation Extended State Observer (ESO) (used in ADRC controller)

Introduction

Active Disturbance Rejection Control (ADRC) is a control method that estimates and compensates for unknown disturbances and system uncertainties in real time. It uses an extended state observer (ESO) to treat disturbances as an additional state, improving robustness and tracking performance without requiring an accurate system model.

From DC Motor Model to General Form

The mechanical equation of a DC motor is given by:

$$J\dot{\omega} = -b\omega + K_t i - T_L \tag{2.15}$$

Dividing by J gives:

$$\dot{\omega} = -\frac{b}{J}\omega + \frac{K_t}{J}i - \frac{1}{J}T_L \tag{2.16}$$

We define a simplified control input u such that the system can be rewritten as:

$$\dot{y} = f(y,t) + b_0 u \tag{2.17}$$

where $y = \omega$ and $b_0 = \frac{K_t}{J}$.

The term $f(y,t)$ represents all unknown dynamics:

$$f(t) = -\frac{b}{J}\omega - \frac{1}{J}T_L + \text{uncertainties} \tag{2.18}$$

Extended State Representation

We define the following states:

$$x_1 = y, \quad x_2 = \dot{y}, \quad x_3 = f(t) \tag{2.19}$$

Thus, the extended state vector is:

$$x = \begin{bmatrix} x_1 \\ x_2 \\ x_3 \end{bmatrix} = \begin{bmatrix} y \\ \dot{y} \\ f(t) \end{bmatrix} \tag{2.20}$$

Augmented System Model

The system dynamics become:

$$\dot{x}_1 = x_2 \tag{2.21}$$

$$\dot{x}_2 = x_3 + b_0 u \tag{2.22}$$

$$\dot{x}_3 = \dot{f}(t) \tag{2.23}$$

We assume:

$$\dot{f}(t) \approx 0 \tag{2.24}$$

This assumption models the disturbance as slowly varying. From eso-reference: The disturbance is modeled as an additional state with bounded or slow dynamics.

Extended State Observer Design

The observer estimates the states:

$$\hat{x}_1, \quad \hat{x}_2, \quad \hat{x}_3 \tag{2.25}$$

The ESO equations are:

$$\dot{\hat{x}}_1 = \hat{x}_2 + \beta_1(y - \hat{x}_1) \tag{2.26}$$

$$\dot{\hat{x}}_2 = \hat{x}_3 + b_0 u + \beta_2(y - \hat{x}_1) \tag{2.27}$$

$$\dot{\hat{x}}_3 = \beta_3(y - \hat{x}_1) \tag{2.28}$$

Interpretation of the Observer

The correction term $(y - \hat{x}_1)$ represents the estimation error.

The gains:

- β_1: corrects output estimation
- β_2: stabilizes dynamic estimation
- β_3: estimates total disturbance

2.3.3 Gain Design of ESO

The gains are chosen based on observer bandwidth ω_o:

$$\beta_1 = 3\omega_o \tag{2.29}$$

$$\beta_2 = 3\omega_o^2 \tag{2.30}$$

$$\beta_3 = \omega_o^3 \tag{2.31}$$

These values correspond to the desired characteristic polynomial:

$$(s + \omega_o)^3 \tag{2.32}$$

gains are derived from bandwidth-based pole placement.

Effect of the Bandwidth

- Small ω_o: smooth but slow estimation
- Large ω_o: fast but noisy estimation

The ADRC observer gains, computed using the bandwidth $\omega_o = 50\,\text{rad/s}$, are given as:

$$l_1 = 30.0690$$

$$l_2 = -32.5189$$

$$l_3 = -4.2398$$

These gains are used in the ADRC observer to ensure accurate disturbance estimation and improved dynamic performance.

Control Law in ADRC

Once the disturbance is estimated, the control input is:

$$u = \frac{u_0 - \hat{x}_3}{b_0} \tag{2.33}$$

where u_0 is a nominal controller.

This results in disturbance cancellation in real time.

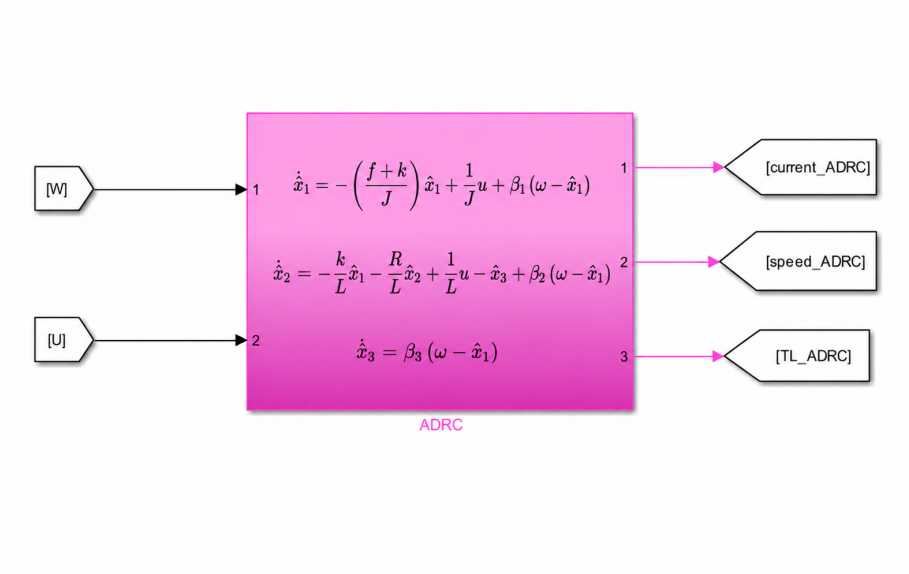


Figure 2.3: ESO MATLAB design

2.3.4 Mathematical Formulation of Sliding Mode Observer (SMO)

Sliding Mode Observer (SMO) is a state estimation technique based on sliding mode principles. It reconstructs unknown system states by injecting a discontinuous correction term, which forces the estimation error to converge to zero, providing strong robustness against disturbances and model uncertainties.

System Representation

Consider a general nonlinear system described by:

$$\dot{x} = Ax + Bu + d(t) \tag{2.34}$$

$$y = Cx \tag{2.35}$$

where $x \in \mathbb{R}^n$ is the state vector, u is the control input, y is the measured output, and $d(t)$ represents unknown disturbances.

Sliding Mode Observer Structure

The Sliding Mode Observer is designed as:

$$\dot{\hat{x}} = A\hat{x} + Bu + L(y - \hat{y}) + G\,\text{sign}(y - \hat{y}) \tag{2.36}$$

where $\hat{x}$ is the estimated state vector, L is the observer gain matrix, G is the sliding gain matrix, and $\text{sign}(\cdot)$ is the discontinuous switching function.

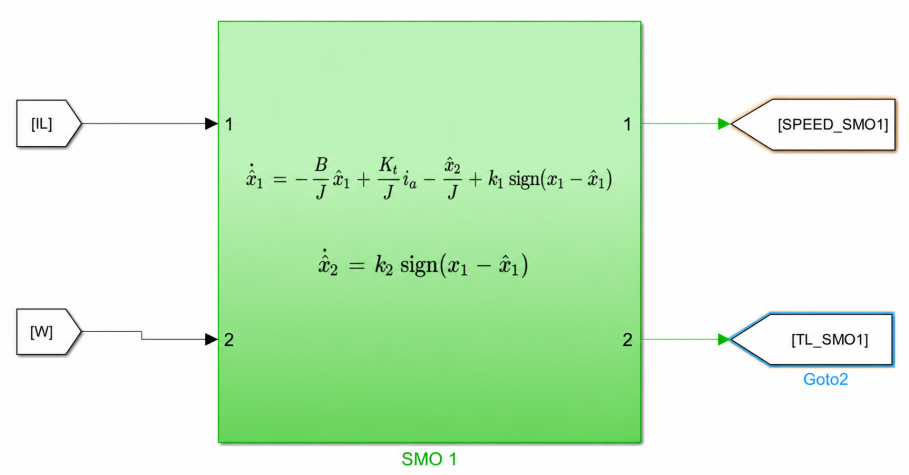


Figure 2.4: Sliding Mode MATLAB design

Observer Interpretation

The SMO consists of two main components. The first term, $L(y - \hat{y})$, represents a linear correction similar to that used in classical observers. The second term, $G\,\text{sign}(y - \hat{y})$, introduces a nonlinear discontinuous action that enhances robustness against disturbances and uncertainties.

This switching term forces the estimation error to reach a sliding surface and remain on it, ensuring convergence.

Estimation Error Dynamics

Define the estimation error as:

$$e = x - \hat{x} \tag{2.37}$$

The error dynamics are given by:

$$\dot{e} = (A - LC)e - G\,\text{sign}(e) \tag{2.38}$$

The discontinuous term drives the estimation error to zero in finite time, even in the presence of bounded disturbances.

Chattering Phenomenon

One of the main drawbacks of sliding mode techniques is the chattering phenomenon, caused by the discontinuity of the sign function. This results in high-frequency oscillations that may affect system performance.

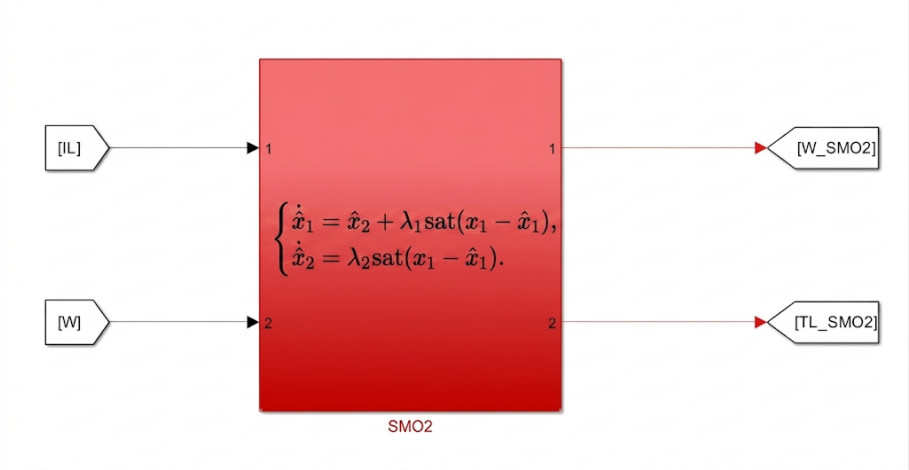


Figure 2.5: Sliding Mode Extreme MATLAB design

2.3.5 Super-Twisting Sliding Mode Observer (ST-SMO)

Introduction

The **Mathematical Formulation of Super-Twisting Sliding Mode Observer (ST-SMO)** is an improved version of the conventional Sliding Mode Observer designed to estimate system states with higher accuracy and robustness. It is based on higher-order sliding mode theory and reduces the chattering effect while maintaining strong disturbance rejection and robustness against model uncertainties.

System Representation

Consider a nonlinear system represented by:

$$\dot{x} = Ax + Bu + d(t) \tag{38.2}$$

$$y = Cx \tag{39.2}$$

where $x \in \mathbb{R}^n$ is the state vector, u is the control input, y is the measured output, and $d(t)$ represents unknown disturbances.

Super-Twisting Observer Structure

The ST-SMO is formulated as:

$$\dot{\hat{x}} = A\hat{x} + Bu + L(y - \hat{y}) + \nu \tag{40.2}$$

where $\hat{x}$ is the estimated state vector, L is the observer gain matrix, and ν is the super-twisting correction term given by:

$$\nu = -k_1 |e|^{1/2} \text{sat}(e) + z \tag{41.2}$$

$$\dot{z} = -k_2 \, \mathrm{sat}(e) \tag{42.2}$$

where k_1 and k_2 are positive observer gains.

Observer Interpretation

The ST-SMO combines a linear correction term with a nonlinear super-twisting action to improve estimation performance. Compared to the classical SMO, it provides smoother convergence of the estimation error and significantly reduces chattering while preserving robustness against disturbances.

Estimation Error Dynamics

The estimation error is defined as:

$$e = x - \hat{x} \tag{43.2}$$

with dynamics expressed as:

$$\dot{e} = (A - LC)e - \nu \tag{44.2}$$

The super-twisting algorithm ensures fast and finite-time convergence of the estimation error, even under bounded disturbances.

Chattering Reduction

A major advantage of the ST-SMO is its reduced chattering effect. By replacing the discontinuous switching action with a smoother higher-order correction, the observer produces more stable estimation signals and improves practical system performance. Problem Statement

2.4 Simulation Framework

The simulation is based on a mathematical model of an armature-controlled DC motor implemented in a numerical computing environment. The system operates in open-loop with a step voltage input, and load torque disturbances are applied to evaluate the dynamic response. A fixed step size is used to ensure stable and accurate simulation results. Table 2.1

Table 2.1: DC Motor Parameters

Parameter	**Symbol**	**Value**	**Unit**
Armature Resistance	R_a	3.5	Ω
Armature Inductance	L_a	0.29	mH
Back-EMF Constant	K_e	1.205	V·s/rad
Torque Constant	K_t	1.205	N·m/A
Rotor Inertia	J	0.002	kg·m^2
Viscous Friction Coefficient	B	0.001	N·m·s/rad
Nominal armature Voltage	V_{dc}	220	V
Nominal armature current	I_{dc}	9	A
Nominal speed	W	1500	rpm
Nominal power	P	1500	W

Load Torque Estimation Performance Analysis

The comparative analysis of the implemented observers shows that all methods are capable of estimating the load torque and rejecting external disturbances; however, clear differences are observed in their dynamic performance, robustness, and estimation accuracy.

The ADRC observer demonstrates a fast and well-balanced response, with a rise time of approximately 0.2 s and a disturbance rejection time in the range of 0.15 to 0.20 s. It provides high robustness against parameter uncertainties and external disturbances, while maintaining a steady-state estimation error below 1% and transient deviations below 2%. These results confirm its strong capability for accurate and stable estimation under varying operating conditions.

The Luenberger observer presents slower dynamics compared to the other methods, with a response time of approximately 0.3 s and a recovery time of 0.25 to 0.30 s after load variations. The steady-state error is around 2% to 3%, and transient deviations reach 3% to 5%. In addition, its performance is highly dependent on the accuracy of the mathematical model, which reduces its robustness under sudden load changes and parameter uncertainties.

The sliding mode observers (SMO1 and SMO2) exhibit the best dynamic performance overall. Both observers reach steady state within approximately 0.10 to 0.15 s and show strong disturbance rejection capability with transient deviations below 2% for SMO1 and below 1% for SMO2. They also demonstrate very high robustness against disturbances and system uncertainties.

However, SMO1 suffers from noticeable chattering, estimated at approximately 5% to 7%, which slightly degrades the smoothness of the estimation signal. In contrast, SMO2 significantly reduces this effect to approximately 2% to 3%, while also achieving a steady-state error below 0.5%, resulting in a smoother and more accurate estimation.

Overall, SMO2 provides the best trade-off between fast response, robustness, and estimation accuracy. ADRC follows as a strong alternative with stable and accurate performance, while the Luenberger observer shows the lowest dynamic performance among the implemented methods. Figure 2.6 and 2.7 is illustration of Tracking Torque and Torque Errors

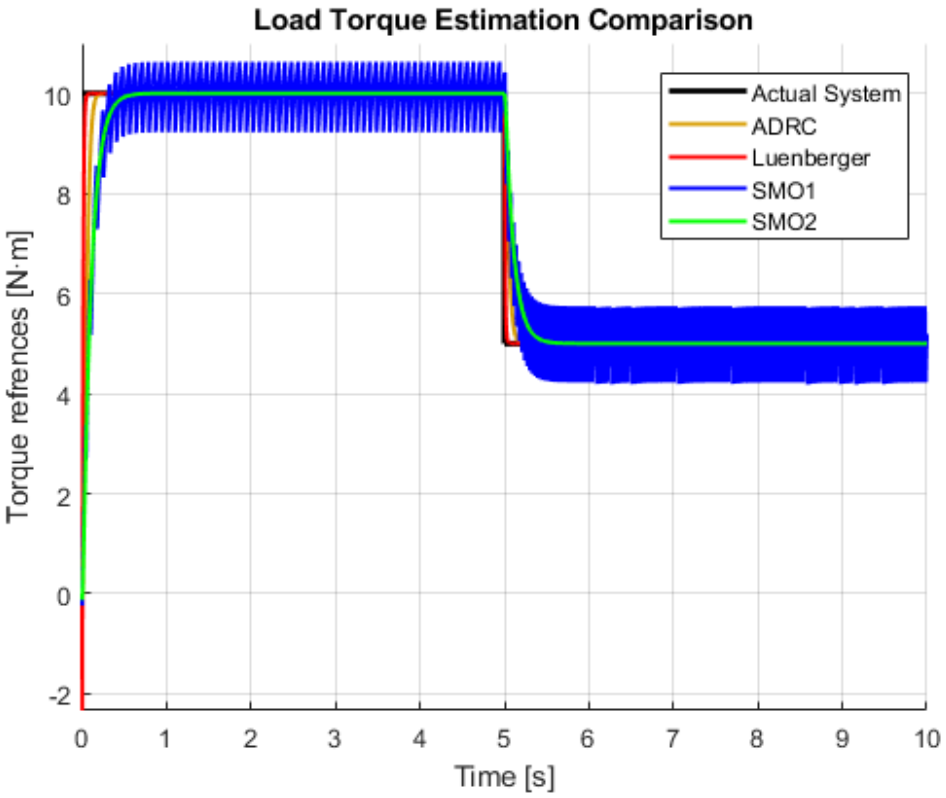


Figure 2.6: Tracking Torque Load in open-loop

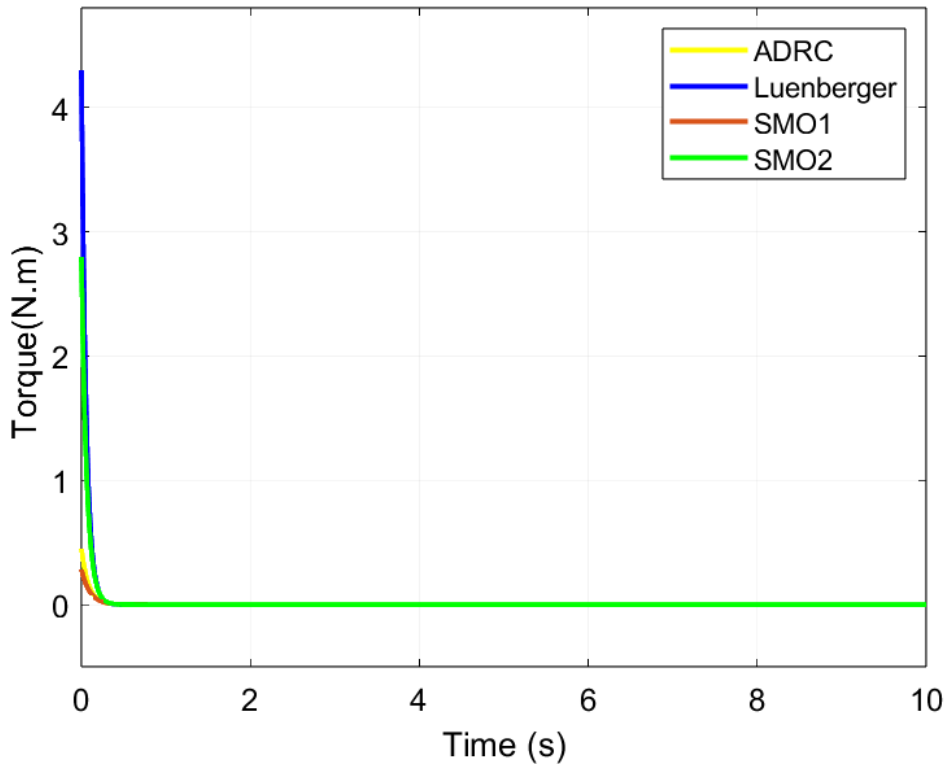


Figure 2.7: Torque Error

2.5 Robustness Evaluation of Load Torque Observers Under Motor Parameter Variations

To evaluate the robustness of the observer/controller, parameter variations were introduced in the DC motor model, specifically affecting the resistance R, inductance L, torque constant K, inertia J, and viscous friction coefficient F. The nominal motor parameters used in the simulation are summarized as follows.

2.5.1 Sumilation Results

Robustness Analysis Under Variations in Armature Resistance 'R':

A parametric analysis is performed by varying the observer gain R in order to evaluate its impact on system performance. The comparison focuses on transient response, steady-state accuracy, and robustness against oscillations and chattering phenomena across the considered observers

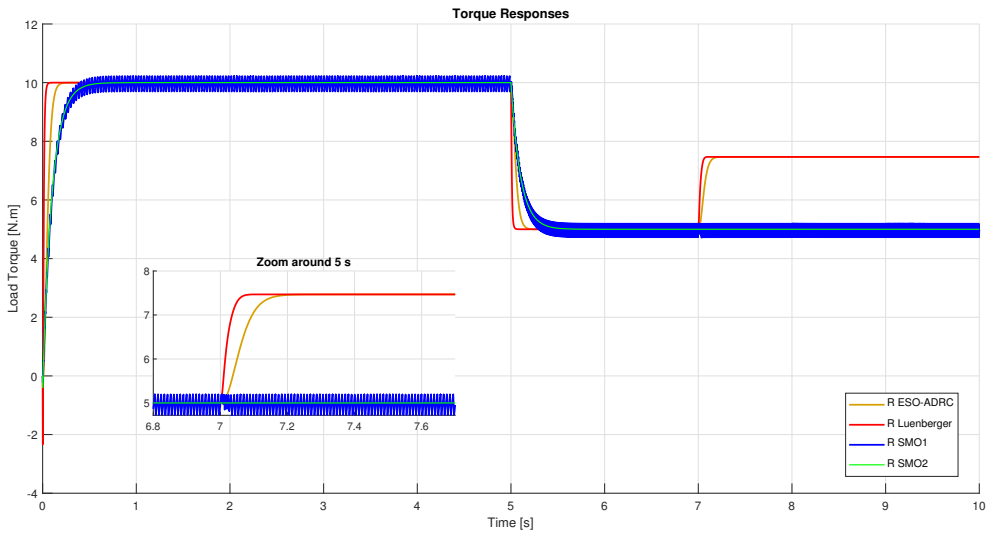


Figure 2.8: Simulink Analysis of R Parameter Variation

Table 2.3: Comparative Performance Analysis of Torque Estimation Methods

Observer	**Chattering / Oscillation**	**Response Time (Temps de réponse)**	**Estimation / Tracking Error**
R_ADRC (Yellow)	None (**0% ripple**, amplitude = **0 N·m**).	Moderate: Slower than Luenberger, with a lag during the **5 s** transition. Settling time is about **15–20%** slower, reaching steady state in **0.15–0.20 s**.	Very low: Clean steady-state tracking with nearly **0% static error**, settling accurately at **10 N·m** and **5 N·m**.
R_LUENBERGER (Red)	None (**0% ripple**, amplitude = **0 N·m**).	Fastest: Immediate response at **0 s** and fastest tracking at **5 s**, with **0% delay** and a rise time of approximately **0.05 s**.	Low: Small transient error of **2–3%** (about **0.2–0.3 N·m**) during the **5 s** step change, then converges accurately.
R_SMO1 (Blue)	Very high chattering: Oscillations of approximately ±0.7 **N·m**, corresponding to **7–14% ripple** relative to **10 N·m** and **5 N·m** operating levels.	Fast: Reaches the target in about **0.05 s**, but does not fully settle because of continuous high-frequency oscillations.	High ripple error: Steady-state oscillations remain around **7%**, varying between **9.3–10.7 N·m** and **4.3–5.7 N·m**.
R_SMO2 (Green)	Negligible chattering: Ripple reduced to nearly **0%**, with amplitude close to **0 N·m**.	Moderate-fast: About **5–10%** slower than Luenberger, with smooth settling in **0.08–0.10 s**.	Low: Stable tracking with less than **1%** steady-state error, accurately following **10 N·m** and **5 N·m** references.

Comparative Analysis for ' L' :

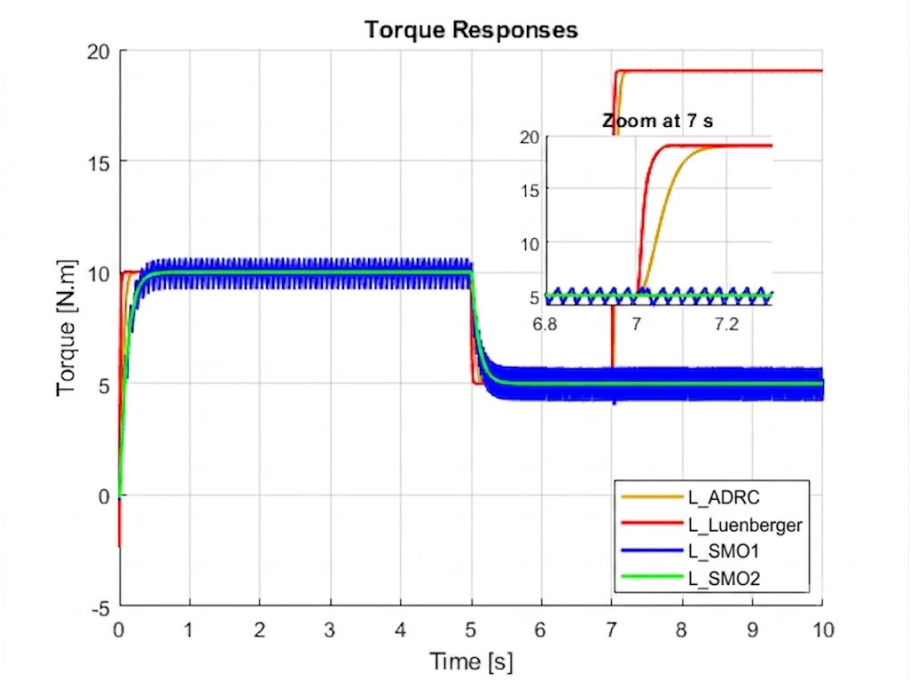


Figure 2.9: Simulink Analysis of L Parameter Variation

Table 2.4: Combined Observer Performance Comparison

Observer / Control Strategy	**Chattering / Oscillations**	**Response Time (at 0 s & 7 s)**	**Tracking / Steady-State Error**
Luenberger (Red)	**0% (None).** Completely smooth signal with no oscillations.	**Fastest (0% delay).** Reaches $19\,\mathrm{N\cdot m}$ at $t = 7\,\mathrm{s}$ in less than $0.05\,\mathrm{s}$, responding almost instantly.	**0% error.** Tracks all reference steps accurately with no steady-state offset.
L_ADRC (Yellow)	**0% (None).** Smooth response without chattering.	**100% (Slowest / Baseline).** Shows a small transient lag and settles about $0.15-0.20\,\mathrm{s}$ after the step at $t = 7\,\mathrm{s}$.	**~1–2% error.** Very low tracking error with stable convergence and near-zero steady-state offset.
L_SMO1 (Blue)	**100% (Highest / Critical).** Severe chattering with oscillations of about $\pm 0.7\,\mathrm{N\cdot m}$ ($\approx 1\,\mathrm{N\cdot m}$ peak-to-peak).	**~10% (Fast).** Rapid convergence, but the response is masked by continuous oscillations.	**~5% error.** Mean value follows the reference, but oscillations cause large instantaneous errors.
L_SMO2	**~5% (Negligible).** Chattering is nearly eliminated, producing a stable signal.	**~10% (Moderately Fast).** Maintains fast sliding-mode dynamics with a startup settling time of about $0.4\,\mathrm{s}$.	**0% error.** Smoothly tracks the reference with excellent steady-state accuracy.

Comparative Analysis for ' K ':

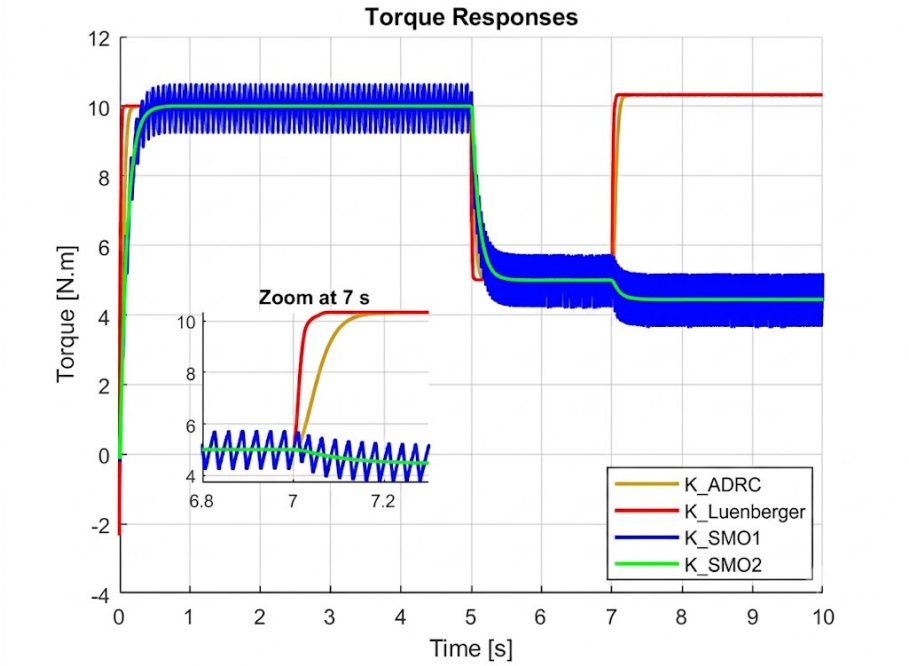


Figure 2.10: Simulink Analysis of K Parameter Variation

Table 2.5: Comparison of Observer Performance

Observer	Chattering Level	Response Time Performance	Tracking / Steady-State Error	Overall Evaluation
K_ADRC	**100% (No chattering)**. Smooth signal, no ripples.	**85%**. Slowest; settles in 0.15 s after the step at $t = 7$ s, near 7.15 s.	**98%**. Zero static error; accurately reaches $10\,\mathrm{N \cdot m}$, $5\,\mathrm{N \cdot m}$, and $10.3\,\mathrm{N \cdot m}$.	Robust and very smooth, with slightly slower transients.
K_Luenberger	**100% (No chattering)**. Completely smooth transition.	**100% (Fastest)**. Reaches $10.3\,\mathrm{N \cdot m}$ within 0.05 s after the step at $t = 7$ s.	**95%**. Zero static error; accurately tracks all references.	Fastest and smoothest, but less robust to disturbances than ADRC.
K_SMO1	**20% (Severe chattering)**. Persistent oscillations of $\pm 0.7\,\mathrm{N \cdot m}$.	**75%**. Fast rise, but heavily affected by oscillations.	**60%**. High error; misses the step at $t = 7$ s and remains near $4.5\,\mathrm{N \cdot m}$.	Classical SMO with strong chattering and poor tracking.
K_SMO2	**90% (Reduced chattering)**. No visible chattering; SMO1 oscillations removed.	**80%**. Moderate response; settles in about 0.4 s at startup.	**95%**. Zero static error before $t = 7$ s, then settles near $4.5\,\mathrm{N \cdot m}$ after the step.	Enhanced SMO with low chattering and good robustness.

Comparative Analysis for ' F ':

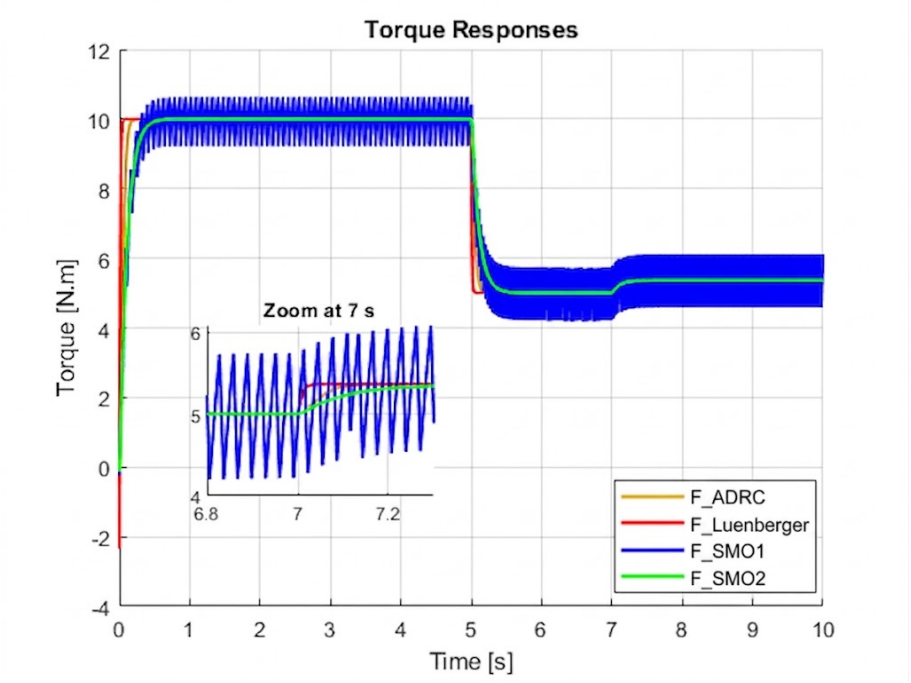


Figure 2.11: Simulink Analysis of F Parameter Variation

Table 2.6: Comparison of Force Estimation Strategies

Strategy	**Chattering Level (Ripple %)**	**Response Time (t_r to $10\,\mathrm{N\cdot m}$)**	**Steady-State Tracking Error**
F_ADRC	0% (Virtually none), providing a smooth force estimate.	Fastest ($\sim 0.15\,\mathrm{s}$), with rapid convergence.	Very low error with stable and smooth tracking.
F_Luenberger	0% (Virtually none), with a smooth estimated signal.	Ultra-fast ($\sim 0.10\,\mathrm{s}$), but with an initial undershoot of about $-2\,\mathrm{N\cdot m}$.	Small tracking offset during step changes (e.g., at 5 s and 7 s).
F_SMO1	High ($15\% - 20\%$), causing noticeable high-frequency oscillations.	Moderate ($\sim 0.25\,\mathrm{s}$), slower than ADRC and Luenberger.	Larger tracking error due to persistent ripple around the reference.
F_SMO2	Very low ($< 1\%$), with chattering significantly reduced.	Moderate ($\sim 0.25\,\mathrm{s}$), similar to SMO1.	Excellent tracking accuracy with high-frequency ripple effectively eliminated.

Comparative Analysis for ' J ' :

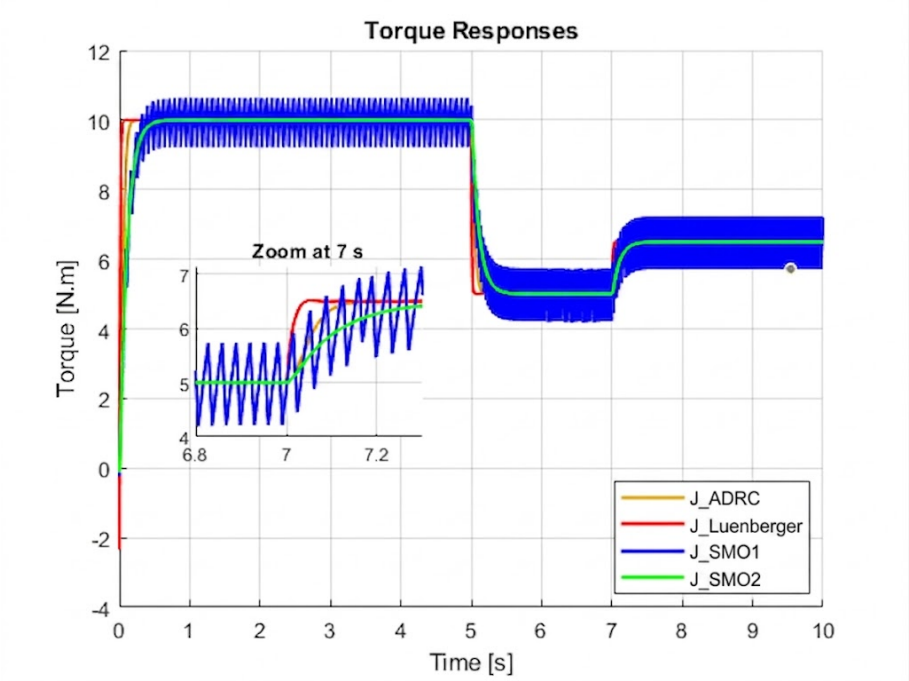


Figure 2.12: Simulink Analysis of J Parameter Variation

Table 2.7: Comparison of J Estimation Strategies

Strategy	**Chattering / Ripple**	**Response Time** (t_r)	**Tracking Error** (e_{ss}) **(Values & %)**
J_ADRC (Orange)	**(0%)**. Perfectly smooth with no oscillations.	**0.03 s**. Fastest response; reaches **10** almost immediately at $t = 0$ s.	**< 0.05 (<0.5%)**. Very accurate; follows the **10**, **5**, and **6.5** steps closely.
J_Luenberger	**(0%)**. Smooth signal with no chattering.	**0.05 s**. Very fast; settles to **6.5** by $t = 7.05$ s.	**< 0.05 (<0.5%)**. No steady-state error after the transient.
J_SMO1	**(~12%)**. Strong chattering; oscillates between **9.4** and **10.6**.	**0.06 s**. Fast response, but the oscillations make it unstable.	**0.6 (~6%)**. Average tracking is good, but the instantaneous error is large.
J_SMO2 (Green)	**0.05 (<0.5%)**. Chattering is reduced by **95%** compared to SMO1.	**0.25 s**. **400%** slower than Luenberger; reaches the target from $t = 7.0$ s to $t = 7.25$ s.	**0.4 (~6%)** during transitions. Temporary lag, then drops to **<1%** at steady state.

2.6 Experimental Validation of Luenberger Observer and Extended State Observer (ESO)

This section presents the experimental validation of the proposed Luenberger Observer and Extended State Observer (ESO) for load torque estimation in a DC motor drive

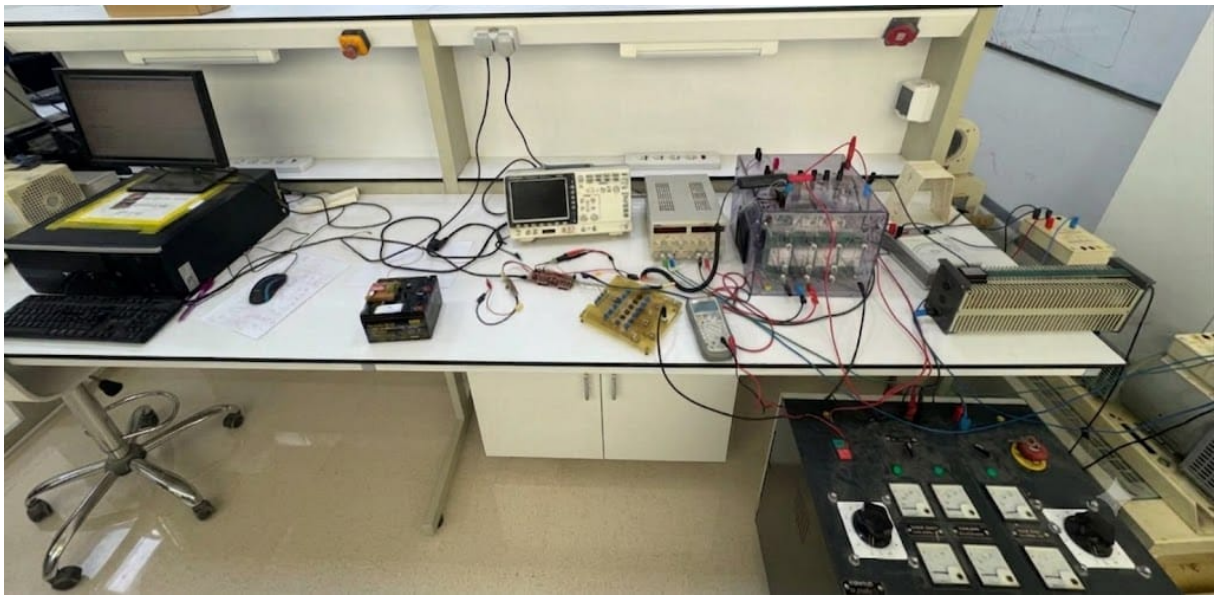


Figure 2.13: Overall Topology

system. The main objective is to evaluate the real-time performance of both observers and to verify their accuracy, robustness, and dynamic behavior under practical operating conditions.

2.6.1 Experimental Test Bench Description

The experimental setup is based on a DC motor drive system equipped with real-time measurement and control capabilities. It is designed to implement and compare both the Luenberger Observer and ESO in real-time.

The test bench includes the following components:

- A separately excited DC motor acting as the main electromechanical system.
- A PWM-based DC drive used to control the armature voltage.
- A real-time control platform STM32 for implementation.
- Current and voltage sensors for electrical measurements.
- An incremental encoder for speed measurement.
- A synchronous generator mechanically coupled to the DC motor is employed as a load emulator. The generator is connected to a variable single-phase resistive load, which allows the creation of controlled electrical loading conditions. By adjusting the resistive load, the electromagnetic torque of the generator is modified, thereby introducing well-defined and repeatable load torque disturbances on the DC motor shaft.

This configuration allows real-time implementation of both observer algorithms and enables accurate performance evaluation under dynamic conditions.

2.6.2 System Modeling and Observation Framework

The DC motor is modeled using standard electrical and mechanical equations, where the load torque is considered as an unknown disturbance.

The state-space representation of the system is used for observer design:

- State variables: armature current and rotor speed.
- Output variable: measured speed.
- Disturbance: unknown load torque.

The Luenberger Observer is designed based on the linear state-space model, while the ESO extends the system by including the total disturbance as an augmented state.

2.6.3 Implementation of Luenberger Observer

The Luenberger Observer is implemented using a discrete-time formulation suitable for real-time execution. The observer gain matrix is selected to ensure fast convergence and stability of the estimation error dynamics.

The estimated states are reconstructed using feedback correction based on the measurement error between actual and estimated outputs.

2.6.4 Implementation of Extended State Observer (ESO)

The ESO is implemented as part of the Active Disturbance Rejection Control (ADRC) framework. It estimates both system states and the total disturbance, which includes load torque and unmodeled dynamics.

The observer is discretized for real-time execution and tuned to achieve a balance between convergence and noise sensitivity.

2.6.5 Experimental Procedure

The experimental tests are conducted under different operating scenarios to evaluate the performance of both observers:

- No-load operation to evaluate steady-state estimation accuracy.
- Step load torque application to test disturbance estimation capability.
- Speed reference changes to evaluate dynamic response.
- Parameter variation scenarios to assess robustness.

During these tests, speed, current, and estimated load torque signals are recorded for analysis.

2.6.6 Results and Discussion

Figures presents the experimental estimation errors associated with the motor speed, estimated load torques, and stator current. The obtained results demonstrate that the proposed observer provides accurate state estimation under varying operating conditions.

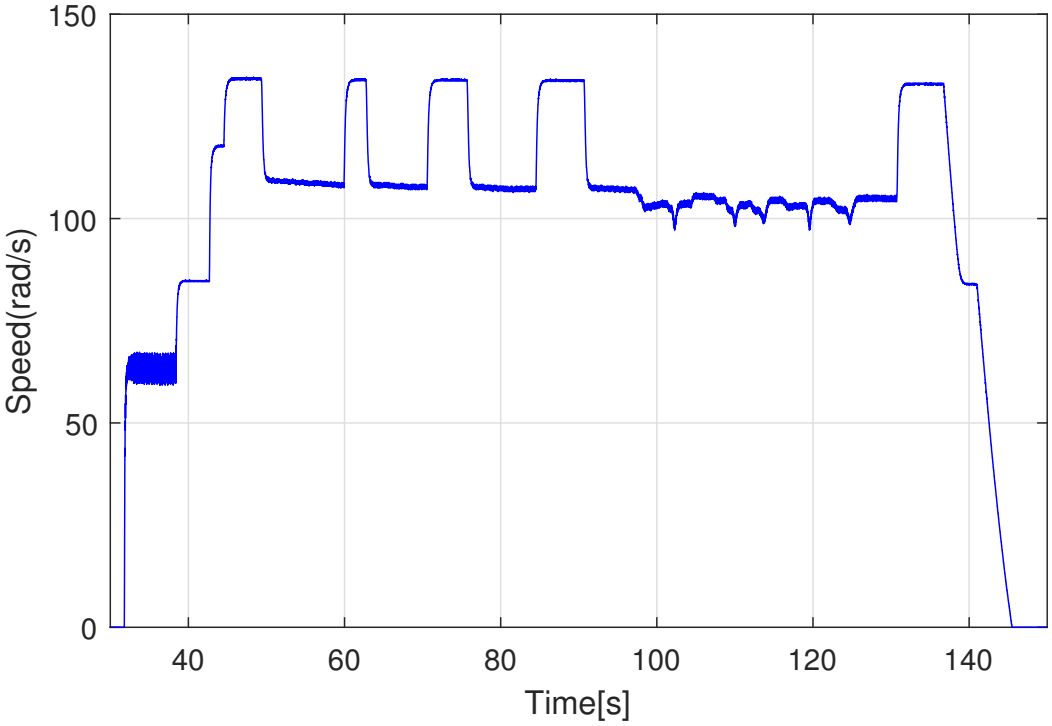


Figure 2.14: EXPERIMENTAL RESULTS : SPEED

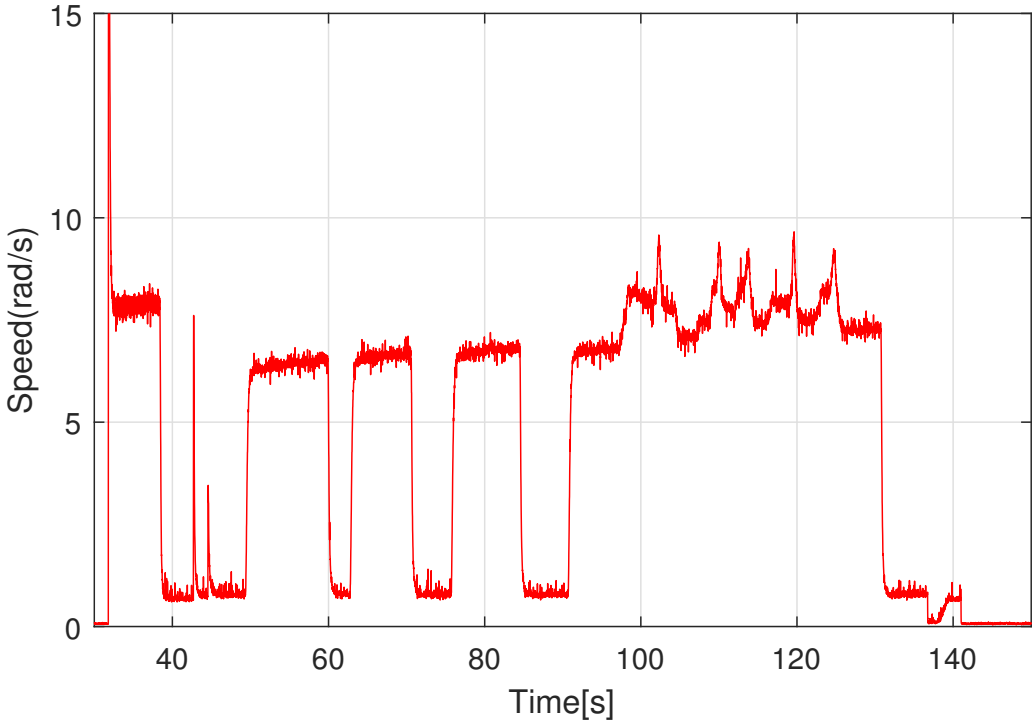


Figure 2.15: EXPERIMENTAL RESULTS : CURRENT

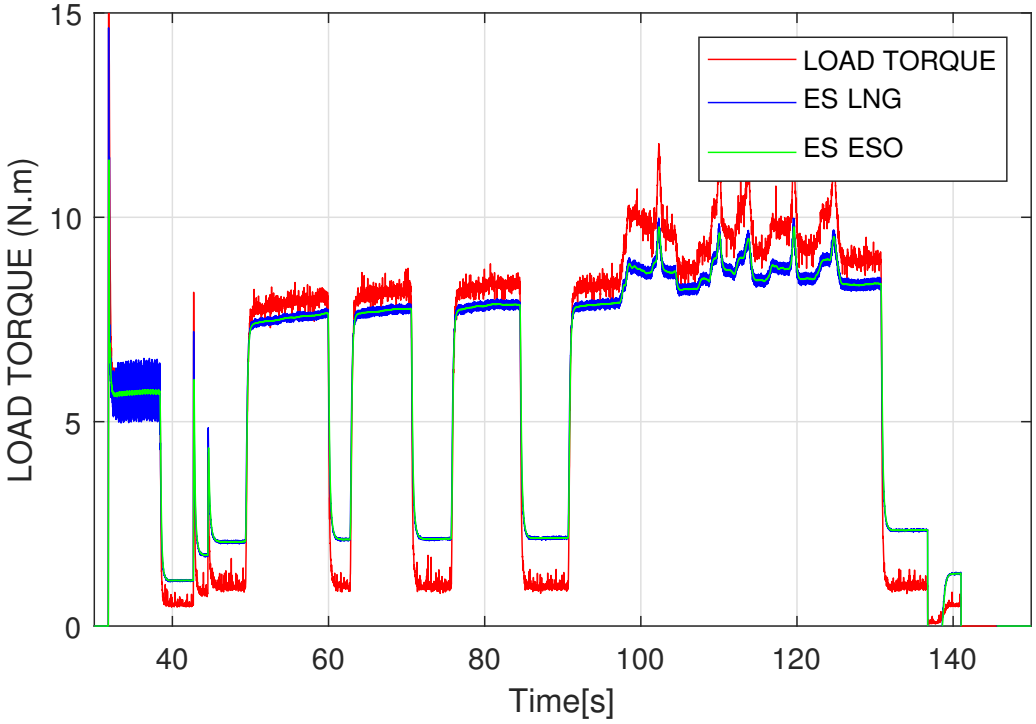


Figure 2.16: EXPERIMENTAL RESULTS : ESTIMATED TORQUES

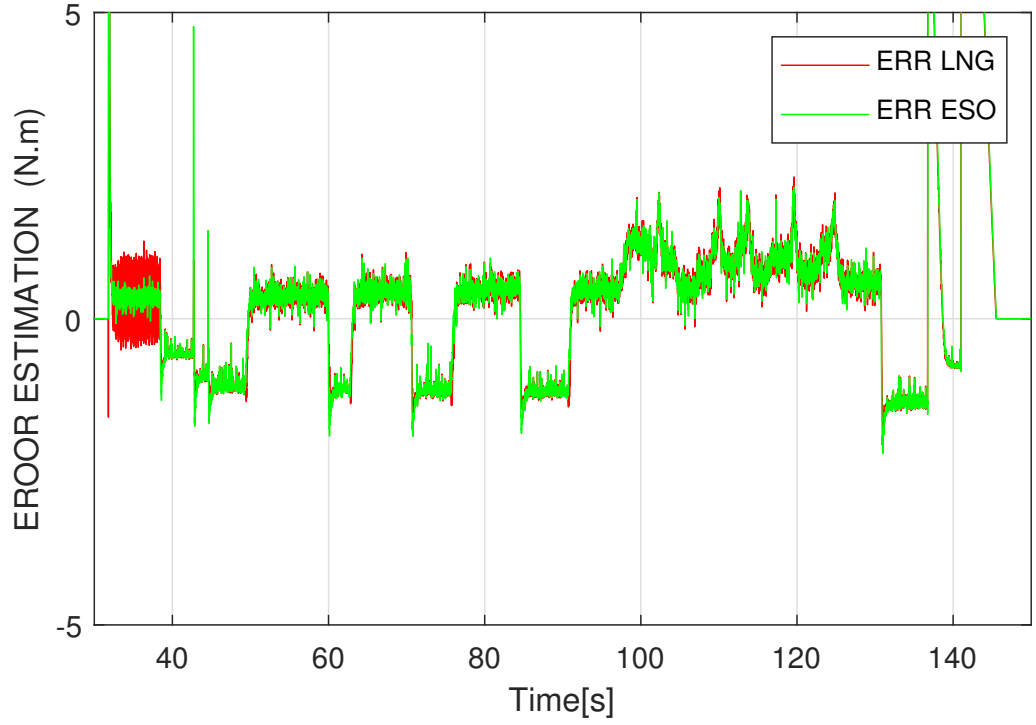


Figure 2.17: EXPERIMENTAL RESULTS : ESTIMATED ERRORS

The experimental results show that both observers are capable of estimating the load torque with acceptable accuracy.

The Luenberger Observer provides fast and stable estimation under nominal conditions. However, its performance may degrade under significant parameter variations due to its dependency on an accurate system model.

In contrast, the ESO demonstrates superior robustness by effectively estimating the total disturbance, including load torque variations and model uncertainties. It provides smoother and more adaptive estimation under varying operating conditions.

2.6.7 Performance Comparison

A comparative analysis between the two observers highlights the following observations:

- Luenberger Observer: fast convergence but sensitive to parameter variations.
- ESO: more robust and adaptive with improved disturbance rejection capability.
- ESO provides better performance under real experimental conditions with uncertainties.

2.6.8 Conclusion of Experimental Validation

The experimental validation confirms the effectiveness of both observers for load torque estimation in DC motor systems. However, the ESO demonstrates superior robustness and adaptability compared to the Luenberger Observer, particularly under disturbance and parameter uncertainty conditions. These results validate the advantage of disturbance estimation-based approaches in practical control applications.

2.7 Conclusion

This chapter presented the mathematical modeling of the armature-controlled DC motor and the analytical development of load torque estimation methods. The motor dynamics were formulated in a state-space representation, and the observability and stability conditions necessary for accurate state estimation were established. Based on this framework, the Luenberger Observer, Sliding Mode Observer, and Extended State Observer (ESO) within the ADRC framework were derived and their estimation principles were discussed.

The open-loop analysis provided a preliminary assessment of the observers' convergence characteristics, estimation accuracy, and ability to reconstruct unknown disturbances and load torque. The results obtained in this chapter establish a solid theoretical foundation for the experimental validation and closed-loop implementation presented in the following chapters.

Chapter 3

Motor Torque Estimation for Disturbance Compensation and Secure Speed Control in Electric Vehicle Applications

3.1 Introduction

Following the observer design and validation presented in the previous chapters, this chapter focuses on the integration of the developed load torque observers into a complete closed-loop DC motor drive system. The primary objective is to evaluate the effectiveness of torque estimation techniques in enhancing speed regulation performance under realistic operating conditions.

To address these issues, a complete DC motor drive architecture is developed, including current and speed control loops as well as the integration of the proposed torque observers. The performance of the control system is assessed through detailed simulations under various operating scenarios. Comparative analyses are carried out with and without torque estimation to highlight the contribution of the observer-based approach.

Finally, the proposed methodology is applied to reduced scale electric vehicle (EV) propulsion system based on a 1.5 kW DC motor. A dynamic model of the vehicle is introduced, and standard driving-cycle conditions are considered to evaluate the behavior of the drive system. The resulting speed, electromagnetic torque, powers and estimated load torque responses are analyzed to demonstrate the practical relevance and effectiveness of the proposed control strategy in real-world EV applications.

3.2 Proposed Topology of the DC Drive

The proposed drive topology is intended to represent a realistic electric vehicle (EV) propulsion system while preserving a sufficiently simple structure for the development and evaluation of speed control and load torque estimation strategies. The propulsion chain consists of a battery pack, an H-bridge power converter, a separately excited DC motor, a reduction gearbox, a driving wheel, and a sensing unit. The overall architecture

is depicted in Figure 3.1.

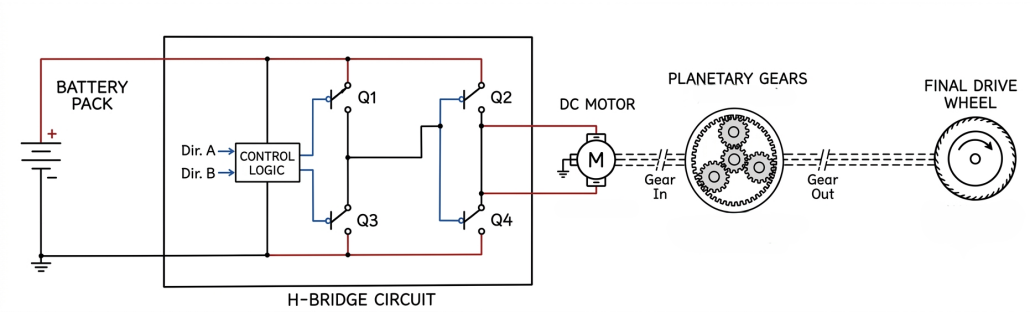


Figure 3.1: Overall topology of the proposed DC motor drive system.

3.2.1 Battery Pack

The battery pack constitutes the primary energy source of the propulsion system. It supplies the DC bus voltage required by the power converter to drive the motor. In this study, the battery is modeled as an ideal DC voltage source with a constant nominal voltage. Battery internal dynamics, state-of-charge variations, and thermal effects are neglected in order to focus on the analysis of the motor drive, control system, and torque estimation performance. In practical EV applications, these functions are supervised by a Battery Management System (BMS), which ensures safe and efficient operation.

3.2.2 H-Bridge Power Converter

The H-bridge converter acts as the interface between the battery and the armature circuit of the DC motor. It consists of four controlled semiconductor switches arranged in a bridge configuration. By means of Pulse Width Modulation (PWM), the converter regulates the average voltage applied to the motor armature and consequently controls the motor speed and electromagnetic torque.

The duty cycle of the PWM signal is generated by the control algorithm according to the speed tracking error, defined as the difference between the reference speed and the measured speed. Assuming ideal switching devices, the average armature voltage can be expressed as

$$V_a = (2 * D - 1) * V_{dc} \tag{3.1}$$

where D denotes the PWM duty cycle ($0 \leq D \leq 1$) and V_{dc} is the battery voltage.

The field winding of the separately excited DC motor is supplied by a constant DC source, ensuring a constant magnetic flux throughout the operating range considered in this work.

3.2.3 DC Motor and Mechanical Transmission

The DC motor converts the electrical energy supplied by the converter into mechanical torque. Owing to its linear characteristics and ease of control, the separately excited DC motor constitutes an appropriate platform for the development and validation of observer-based control strategies.

The generated torque is transmitted to the wheel through a reduction gearbox, which adapts the motor speed to the vehicle requirements while increasing the available traction torque. The vehicle dynamics introduce a load torque resulting from the combined effects of inertia, rolling resistance, aerodynamic drag, and road slope variations. This load torque acts as an external disturbance on the drive system and directly influences the speed regulation performance.

Consequently, accurate estimation of the load torque is essential for implementing disturbance compensation mechanisms and improving the robustness of the propulsion system under varying operating conditions.

.

3.2.4 PWM Generation Unit

The PWM generation unit produces the switching signals required to control the H-bridge converter. It converts the controller output into a PWM signal with a variable duty cycle, allowing regulation of the average voltage applied to the motor armature. By adjusting the duty cycle, the motor speed and electromagnetic torque can be effectively controlled. This unit provides the interface between the control algorithm and the power converter, ensuring accurate and reliable operation of the drive system.

3.2.5 DC Motor

Although Chapter 2 focused on the design and open-loop evaluation of the proposed observers, the objective of the present chapter is to investigate their performance within a closed-loop control framework. The open-loop analysis provided a preliminary assessment of the estimation capabilities of the different observers, allowing their convergence properties, estimation accuracy, and robustness to load disturbances to be evaluated independently of the controller dynamics.

Building upon these results, the observers are now integrated into a complete DC motor drive system incorporating cascaded speed and current control loops. This closed-loop implementation enables the estimated load torque to be utilized for disturbance compensation and performance enhancement. Furthermore, the proposed control architecture is evaluated under operating conditions representative of electric vehicle applications, thereby providing a more realistic assessment of the effectiveness of the observer-based torque estimation strategies.

3.2.6 Sensors

The sensing unit provides the feedback signals required by the control and estimation algorithms. Three types of sensors are employed in this topology:

- **Speed sensor:** An incremental encoder or Hall-effect sensor measures the rotor angular velocity ω (rad/s). This signal serves as the primary feedback variable for the speed control loop.
- **Current sensor:** A shunt resistor or Hall-effect current transducer measures the armature current i_a. The current measurement is used in the inner control loop and also provides the observable output for the torque observer.

- **Voltage sensor:** The terminal voltage V_a is monitored to ensure proper PWM operation and to provide additional state information to the observer.

Together, these measurements constitute the output vector $\mathbf{y}(t) = [i_a,\ \omega]^\top$ fed into the observer and controller blocks.

3.3 Control Scheme

The proposed control strategy is based on a cascaded closed-loop architecture comprising an outer speed control loop and an inner current control loop. This structure is widely adopted in electric drive systems due to its simplicity, robustness, and ability to achieve high-performance speed regulation. The inner current loop provides fast control of the motor electromagnetic torque, while the outer speed loop ensures accurate tracking of the reference speed. Moreover, the cascade arrangement facilitates independent tuning of the control loops and naturally limits the armature current, thereby protecting both the motor and the power converter.

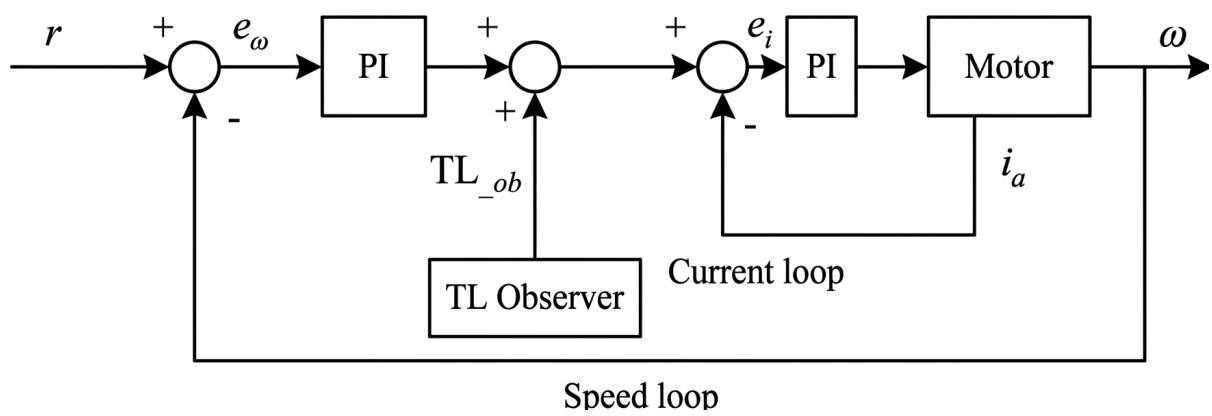


Figure 3.2: Block diagram of the proposed cascaded speed and current control scheme with observer-based with torque estimation.

To enhance disturbance rejection capabilities, the control scheme incorporates the load torque estimated by the observer developed in the previous chapter. The estimated torque is used as a feedforward compensation signal, enabling the controller to counteract load disturbances before significant speed deviations occur. Consequently, the proposed strategy improves speed regulation, reduces transient performance degradation, and increases the robustness of the drive system under varying operating conditions.

The overall control structure is illustrated in Figure 3.2.

3.3.1 Speed Control Loop

The outer loop regulates the motor speed to track a reference speed ω_{ref}. A Proportional-Integral (PI) controller computes the speed error:

$$e_r(t) = \omega_{ref}(t) - \omega(t) \tag{3.2}$$

and generates a reference current i_{ref} as its output:

$$i_{ref}(t) = K_p e_r(t) + K_i \int_0^t e_r(\tau) d\tau \tag{3.3}$$

The gains K_p and K_i are tuned using pole-placement based on the desired closed-loop bandwidth of the speed loop. A saturation block limits i_{ref} to a maximum safe armature current, protecting the power stage and motor windings.

When the torque observer is active, an additional feed-forward compensation term derived from the estimated load torque $\hat{T}_L$ is injected into the speed controller output to proactively counteract disturbances before the speed error grows. This significantly reduces the speed dip following sudden load changes.

Gain Calculation for the Speed Loop

Given a desired speed-loop bandwidth $\omega_{\text{BW,speed}}$ (in rad/s), the PI gains are selected using pole-placement:

$$\omega_{\text{BW,speed}} = 20 \times 2\pi \tag{3.4}$$

$$K_{p,\text{speed}} = \frac{J \cdot \omega_{\text{BW,speed}}}{k} \tag{3.5}$$

$$K_{i,\text{speed}} = \frac{f \cdot \omega_{\text{BW,speed}}}{k} \tag{3.6}$$

where J is the rotor inertia, f is the viscous friction coefficient, and k is the torque constant.

3.3.2 Current Control Loop

The inner loop controls the armature current i_a to track the reference i_{ref} generated by the speed controller. A fast PI current controller computes the current error:

$$e_i(t) = i_{ref}(t) - i_a(t) \tag{3.7}$$

and produces the reference armature voltage V_{ref}:

$$V_{ref}(t) = K_p e_i(t) + K_i \int_0^t e_i(\tau) d\tau \tag{3.8}$$

This voltage command is translated into a PWM duty cycle $D = V_{ref}/V_{dc}$, which drives the H-Bridge gate signals. The current loop bandwidth is designed to be at least five to ten times faster than the speed loop to ensure the cascade separation principle holds.

Gain Calculation for the Current Loop

Select a desired current-loop bandwidth $\omega_{\text{BW,curr}}$ (in rad/s), typically 5–10 times $\omega_{\text{BW,speed}}$:

$$\omega_{\text{BW,curr}} = 200 \times 2\pi \tag{3.9}$$
$$K_{p,\text{curr}} = L \cdot \omega_{\text{BW,curr}} \tag{3.10}$$
$$K_{i,\text{curr}} = R \cdot \omega_{\text{BW,curr}} \tag{3.11}$$

where L is the armature inductance and R is the armature resistance. This choice places the closed-loop current pole near $\omega_{\text{BW,curr}}$, ensuring fast tracking.

3.3.3 Controller Tuning

The PI controller parameters are determined using a pole-placement approach based on the desired closed-loop bandwidths of the speed and current loops. The speed controller is designed to achieve the required mechanical response while ensuring system stability, whereas the current controller is tuned to provide fast current tracking and effective torque control. The resulting bandwidth separation guarantees proper decoupling between the electrical and mechanical dynamics of the drive system.

3.3.4 Observer Integration and Torque Estimation

The observers developed and evaluated in Chapter 2 (ESO, Luenberger, SMO1, and SMO2) are integrated in parallel with the closed-loop controller. Each observer receives the measured current i_a and speed ω as inputs and provides an estimated load torque $\hat{T}_L$ as output. This estimate is used in two ways:

- **Feed-forward compensation:** The estimated disturbance is directly subtracted from the controller output, reducing the burden on the feedback loop and improving transient response. it's more clear in Figure **??**
- **Security monitoring:** The estimated torque is continuously compared against reference torque bounds. Anomalous deviations trigger a safety response, transitioning the drive to a safe operating state.

The integration of the observer within the closed-loop scheme enables a significant reduction in speed recovery time following load disturbances, as demonstrated in the simulation results below.

3.4 Simulation Results

This section presents the performance evaluation of the proposed control strategy through numerical simulations. The objective is to assess the effectiveness of the cascaded PI control structure and to highlight the contribution of observer-based load torque estimation in improving disturbance rejection and speed regulation. The simulation results discussed in this chapter are obtained using the nominal DC motor parameters presented in Chapter 2. These parameters, which were employed for the modeling and observer design procedures, provide the basis for evaluating the dynamic performance, estimation accuracy, and robustness of the proposed load torque observers under various operating conditions.

3.4.1 Simulation Without Torque Estimation

In the first scenario, the closed-loop system operates using only the cascaded PI speed and current controllers, without any load torque estimation or feedforward compensation. The motor is subjected to a step reference speed of 100 rad/s at $t = 0$ s, followed by an additional step to 150 rad/s at $t = 8$ s. A sudden increase in external load torque from 5 N·m to 10 N·m is applied at $t = 5$ s.

The obtained speed response, illustrated in Fig. 3.3, shows that the PI controller ensures satisfactory reference tracking under nominal operating conditions. However, when the load disturbance is applied at $t = 5$ s, a noticeable transient speed deviation occurs. As visible in the zoomed inset, the speed drops to approximately 97–98 rad/s before slowly recovering to the reference, with a settling time of approximately 2–3 s, driven purely by the integral action of the PI speed controller. This highlights the limited disturbance rejection capability of the classical PI-based control structure.

The armature current response shows a significant transient peak following the disturbance. These results motivate the integration of observer-based torque estimation to improve disturbance rejection.

3.4.2 Simulation With Torque Estimation

In the second scenario, observer-based load torque estimation is introduced to enhance the robustness of the control system. Four different observers—ESO (ADRC), Luenberger, SMO1, and SMO2—are implemented to estimate the load torque in real time. The estimated torque is used as a feedforward compensation term within the speed control loop.

The same reference speed profile and load torque disturbance as in the previous case are applied to ensure a fair comparison.

Figures 3.3, 3.4, 3.5 and 3.6 presents the speed, current, speed error, and estimated torque responses obtained with each observer-based compensation strategy. The results clearly demonstrate that the inclusion of torque estimation significantly improves disturbance rejection, reduces speed dips during load variations, and enhances the dynamic performance of the drive system.

Speed Response. As shown in the speed response plot 3.3 and its zoomed inset at $t = 5$ s, all observer-based strategies drastically reduce the speed deviation caused by the load disturbance compared to the uncompensated PI case. The ESO (ADRC), Luenberger, and SMO1 observers achieve near-identical and very tight speed regulation, with a speed dip of less than 1 rad/s and rapid recovery within approximately 0.2–0.3 s. The SMO2 observer exhibits a slightly larger transient deviation and a longer recovery time compared to the other three strategies, as visible in the zoomed region.

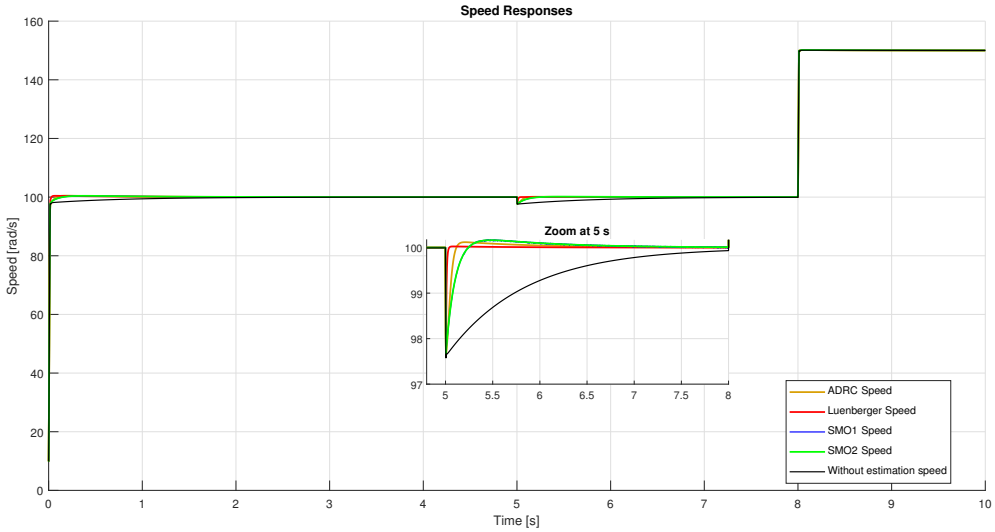


Figure 3.3: Speed responses

Speed Error Response. The error response plot 3.4 confirms these observations. At $t = 5$ s, the ESO (ADRC) and Luenberger observers produce small, well-damped error peaks. The SMO2 strategy generates a noticeably larger error spike—reaching approximately 2.5 rad/s—with a longer settling time of around 1–2 s. A second, more prominent SMO2 error peak of approximately 50 rad/s is observed at $t = 8$ s during the reference speed step change, as highlighted in the zoomed inset. The uncompensated case (black curve) exhibits a sustained, slowly decaying error following the load disturbance, confirming the limited rejection capability of the standalone PI controller.

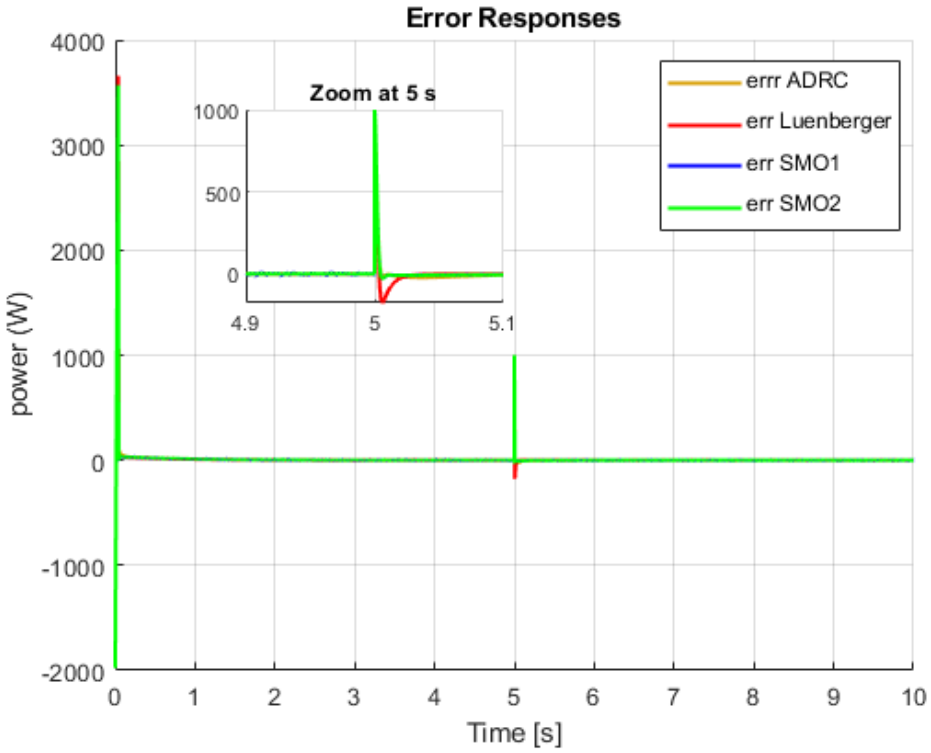


Figure 3.4: Estimation error responses

Current Response. The armature current responses are nearly identical across all observer-based strategies and the uncompensated case during steady-state operation. At the load step ($t = 5$ s), the Luenberger observer induces a small additional transient current spike (visible in the zoomed inset), while the other strategies transition smoothly to the new steady-state current level of approximately 9.5 A. At $t = 8$ s, a sharp current spike occurs for all strategies due to the reference speed step, after which the current settles to a new steady-state value corresponding to the higher speed and load. Look at figure 3.5

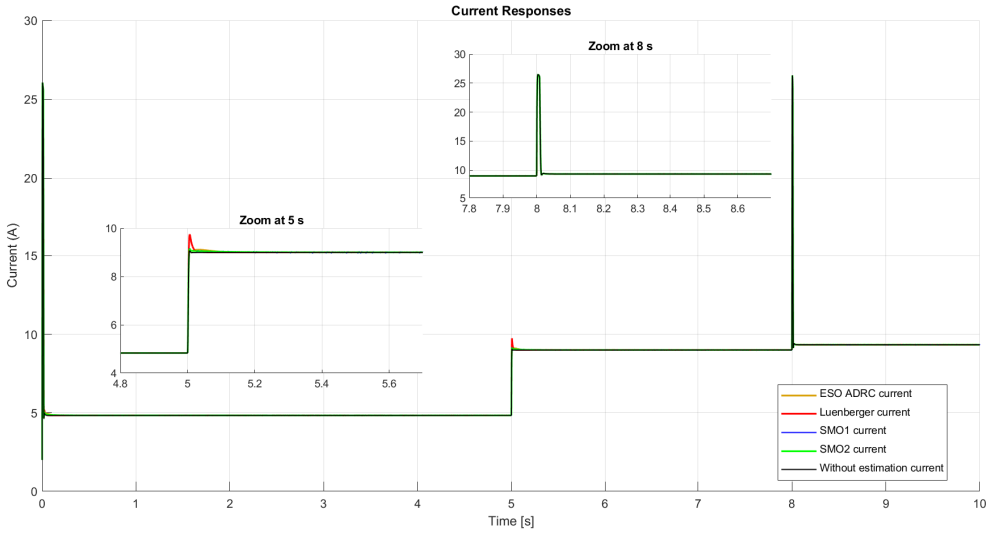


Figure 3.5: Current responses

Torque Estimation. The torque estimation responses reveal meaningful differences between the observers. figure 3.6 The Luenberger observer achieves the fastest convergence to the true load torque value following the step change at $t = 5$ s. The ESO (ADRC) and SMO2 observers exhibit a slightly slower rise, converging to the reference torque within approximately 0.3–0.5 s. The SMO1 observer, while accurately tracking the reference torque in steady state, exhibits persistent chattering oscillations around the true value, which is an inherent characteristic of classical sliding mode approaches. Furthermore, at startup ($t = 0$ s), the Luenberger observer produces an undershoot to approximately -3 N·m before converging to the initial load torque of 5 N·m.

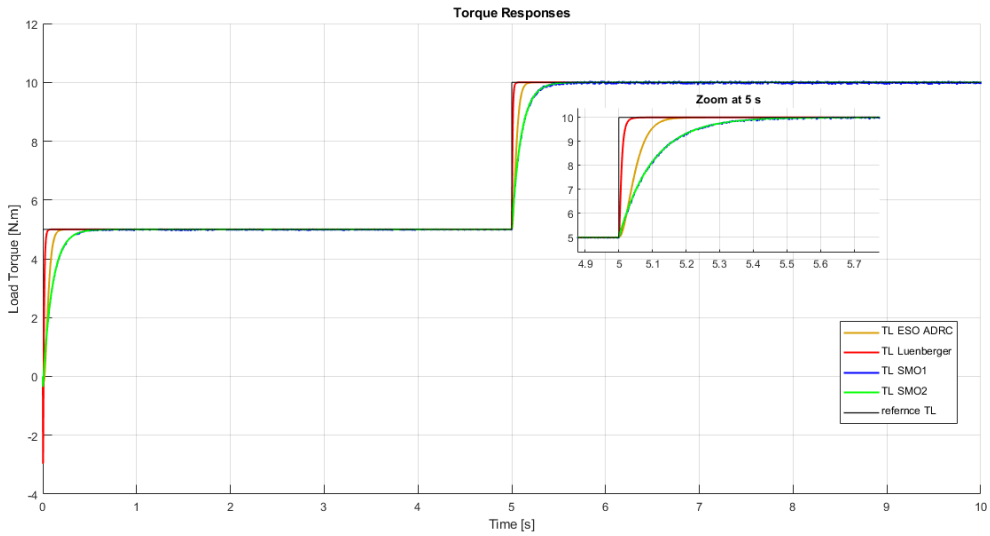


Figure 3.6: Torque estimation responses

Table 3.1 summarizes the closed-loop performance of the DC motor drive system with and without observer-based load torque estimation. The comparison highlights the significant improvements achieved through the integration of torque observers. Without torque estimation, the system exhibits a relatively large speed dip (approximately 2–3 rad/s) and a slow recovery time of about 2–3 s following load disturbances. In contrast, the ESO (ADRC), Luenberger Observer, and SMO1 considerably enhance the dynamic response by reducing the speed deviation to less than 1 rad/s and shortening the recovery time to less than 0.3 s. Regarding estimation accuracy, the Luenberger Observer provides the lowest torque estimation error, while both the Luenberger Observer and SMO1 exhibit the fastest convergence speed. However, the classical Sliding Mode Observer (SMO1) suffers from pronounced chattering effects, which may affect practical implementation. The ESO and Luenberger Observer achieve excellent overall performance, combining high estimation accuracy, rapid disturbance rejection, and smooth operation. Although SMO2 offers reduced chattering and satisfactory estimation performance, its dynamic response remains slightly slower. Overall, the results demonstrate that observer-based torque estimation significantly improves speed regulation, disturbance rejection capability, and system robustness compared with the conventional control strategy.

Table 3.1: Closed-loop performance comparison with and without observer-based torque estimation.

Criterion	**No Observer**	**ESO (ADRC)**	**Luenberger**	**SMO1**	**SMO2**
Speed Dip (rad/s)	∼2–3	<1	<1	<1	∼2
Recovery Time (s)	∼2–3	<0.3	<0.3	<0.3	∼1–2
Chattering	None	None	None	**High**	Low
Torque Estimation Error	N/A	Low	Very Low	Moderate	Low
Torque Convergence Speed	N/A	Moderate	Fast	Fast	Moderate
Overall Performance	Baseline	Excellent	Excellent	Good	Good

3.5 Application to a Real Electric Vehicle Scenario

To assess the practical relevance of the proposed control and estimation strategy, the system is tested under a realistic electric vehicle driving cycle representing actual vehicle operation. In this case, the speed reference is not a simple step input, but a time-varying profile derived from typical urban and suburban driving conditions.

The driving cycle reproduces real operating situations such as vehicle start-up from rest, frequent stop-and-go traffic, gradual acceleration to cruising speed, constant-speed highway driving, and deceleration phases associated with braking and traffic conditions. These variations impose continuously changing torque demands on the drive system due to vehicle inertia, road load, and aerodynamic resistance.

This realistic scenario enables the evaluation of the controller and observer performance under conditions similar to those encountered in an actual electric vehicle. In particular, it allows verification of speed tracking accuracy, robustness against rapid load changes, and the effectiveness of load torque estimation and compensation in improving overall drive behavior. reformulate Real Electric Vehicle Application:

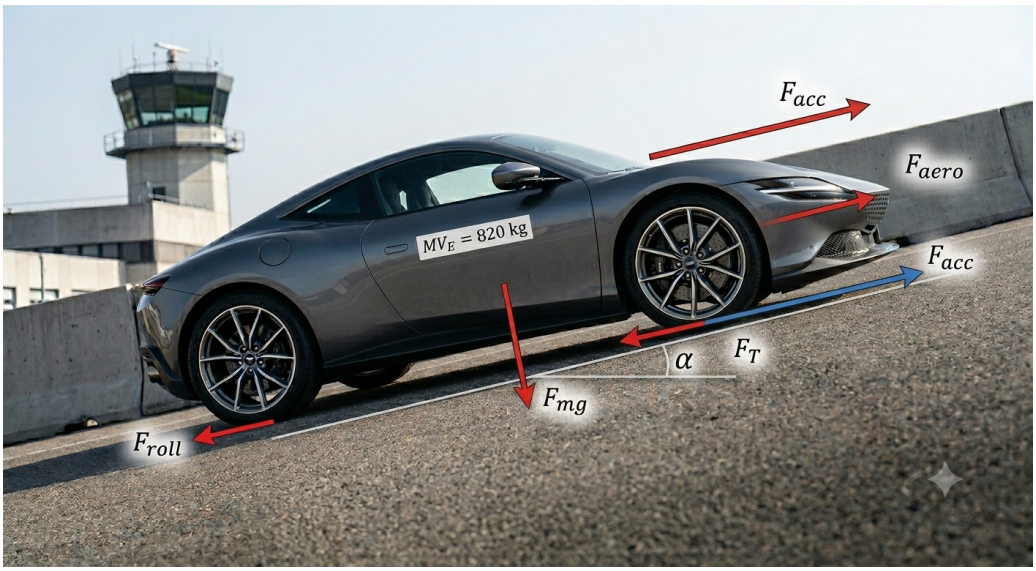


Figure 3.7: Simplified urban driving cycle used as speed reference for the EV simulation.

3.5.1 Dynamic Model of the Electric Vehicle

The longitudinal dynamic model of the electric vehicle is used to compute the load torque profile experienced by the motor during the driving cycle. The EV is modeled as a point mass subject to the following resistive as showen in figure 3.7.:

Since the land vehicles are designed to move primarily in one direction, only single dimensional lateral dynamics are considered. There are five lateral force components: inertial force, longitudinal traction force, air drag, tire rolling resistance, and gravity when the vehicle is moving up or down a hill.

Table 3.2: Parameters of Bluecar type urban electric vehicle

VE Parameters	**Value**
Vehicle mass (M_{VE})	820 kg
Gravity force (g)	9.81 m/s^2
Radius of a wheel (r)	0.33 m
Air density (ρ)	1.2 kg/m^3
Front area (S)	2.75 m^2
Air penetration coefficient (C_x)	0.3
Rolling resistance coefficient in dynamic state (C_0)	1.6×10^{-6}
Rolling resistance coefficient in static state (C_1)	0.008
Incline angle of the road (α)	2.5%

The power at the wheel P_{EV} which can be expressed by:

$$P_{EV} = T_T \Omega_{roll} \tag{3.12}$$

The total traction torque T_T and the rotation speed of the wheel Ω_{roll}:

$$T_T = F_T r \tag{3.13}$$

$$\Omega_{roll} = \frac{V_{ev}}{r} \tag{3.14}$$

With: r the radius of the wheel.

Finally we have:

$$P_{EV} = F_T V_{ev} \tag{3.15}$$

The total force is then written in the following form:

$$F_T = F_{slope} + F_{aero} + F_{roll} + F_{acc} \tag{3.16}$$

A. Rolling Resistance:

As the tire rotates, a part of the tire is continuously depressed at the bottom, and then released back to its original shape after it leaves the contact region. These depressing and releasing processes are not totally elastic. That is, due to the damping action, energy is consumed during the deforming and recovering processes. Such a loss of energy in the tire is reflected as a rolling resistance that opposes the motion of the vehicle. Obviously, the amount of deformation depends on the vehicle's weight. Typically,

$$F_{roll} = M_{ve} g (C_0 + C_1) v_x^2 \tag{3.17}$$

B. Aerodynamic Drag Force :

When a headwind blows at a speed of V_{wind} to a moving vehicle [3], the aerodynamic drag force exerted on a vehicle is calculated as

$$F_{aero} = \frac{\rho C_d A_F}{2} (V_x + V_{wind})^2 \tag{3.18}$$

where ρ is the mass density of air, C_d is the aerodynamic drag coefficient, and A_F is the equivalent frontal area of the vehicle. The mass density of air is equal to $\rho = 1.225$ kg/m^3 at the commonly used standard set of conditions (15°C and a 101.32 kPa).

To investigate the aerodynamic effect separately, we assume in the following that a vehicle is traveling a horizontal road when the headwind is equal to zero. Neglecting the rolling resistance

$$F_{aero} = \frac{\rho C_d A_F}{2}(V_x)^2 \tag{3.19}$$

C. Force due to road profile

The force of the road dynamics is the force of gravity obtained when the vehicle is moving on a sloping road

$$F_{slope} = m_v g \sin\alpha \tag{3.20}$$

D. Force due to acceleration :

The force due to acceleration ensures the dynamic behavior desired by the driver.

$$F_{acc} = m_v \frac{dV_x}{dt} \tag{3.21}$$

IV.5 Transmission and mechanical reducer:

The reducer is a very important element often allowing a consequent saving on the mass of the motor whose dimensions are determined mainly by the torque to be supplied

$$T_T = g_{dr} T_m \tag{3.22}$$

$$\omega_m = \frac{1}{g_{dr}} \omega_{roll} \tag{3.23}$$

g_{dr}: The gear ratio

3.5.2 Driving Cycle

The considered electric vehicle is rated at 40 kW. To adapt the study to the reduced-scale DC motor test platform, the power was scaled to a 1.5 kW motor drive. The corresponding torque reference was limited to 10 N · m, which represents the maximum torque capability of the selected motor. Therefore, all driving-cycle simulations were normalized according to these reduced-scale power and torque limits.

A simplified urban driving cycle is adopted as the speed reference profile. The cycle consists of repeated acceleration–cruise–deceleration sequences representing typical city driving conditions. The reference speed profile is mapped to the motor angular velocity through the vehicle gear ratio and wheel radius.

The New European Driving Cycle (NEDC) is a standardized speed profile historically used to evaluate vehicle performance and emissions under controlled and repeatable conditions. It consists of a sequence of low-speed urban phases followed by an extra-urban

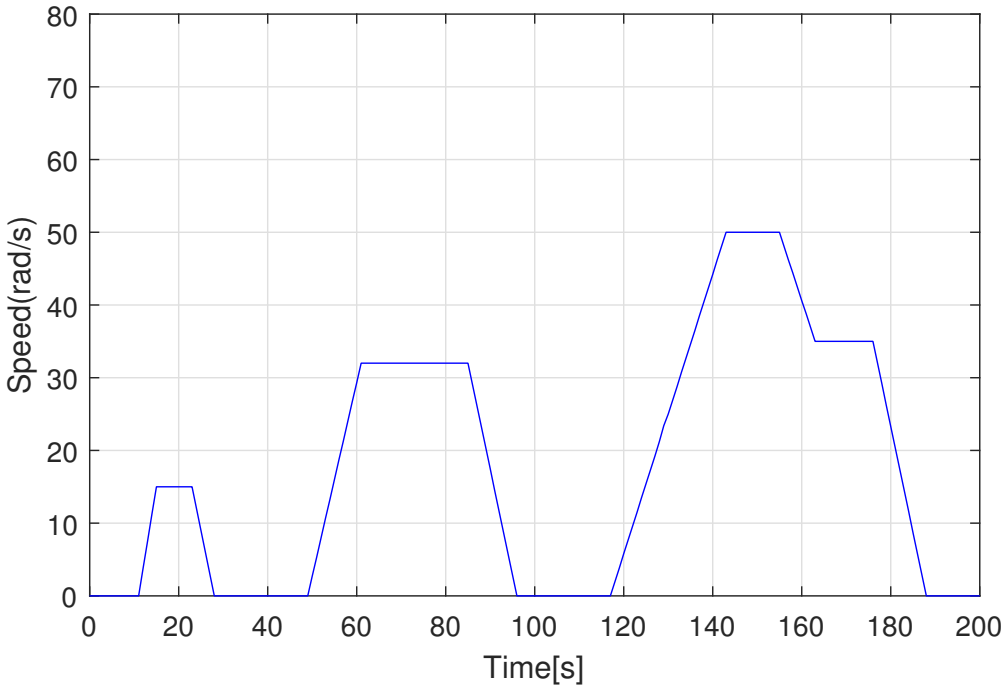


Figure 3.8: URBAN PART OF NEDC DRIVING SYCLE

segment representing highway driving. The cycle includes repeated acceleration, cruising, deceleration, and idle periods, making it suitable for assessing the dynamic behavior of electric vehicle propulsion systems. In this work, the NEDC is used as a realistic reference to validate the speed tracking capability and robustness of the proposed control and torque estimation strategy.

3.5.3 Torque and Speed Profiles

Figures Figure 3.8 illustrate the speed and load torque and power profiles obtained from the reduced-scale dynamic model corresponding to a rated power of 1 kW. The scaling process preserves the dynamic characteristics of the original system while adapting the operating levels to the laboratory prototype. As observed, the speed profile follows the prescribed reference trajectory with smooth transitions between operating points, whereas the torque profile exhibits the expected transient peaks during acceleration and deceleration phases before settling to the values required by the load conditions. These results confirm that the reduced-scale model accurately reproduces the fundamental dynamic behavior of the propulsion system and provides a suitable basis for subsequent control and experimental investigations.

Figure 3.12 illustrates the motor speed response during the electric vehicle driving cycle. The results show that the actual speed closely follows the reference profile throughout all operating phases, including acceleration, cruising, and deceleration. This confirms the effectiveness of the cascaded control structure in ensuring accurate speed tracking under time-varying load conditions representative of real driving operation.

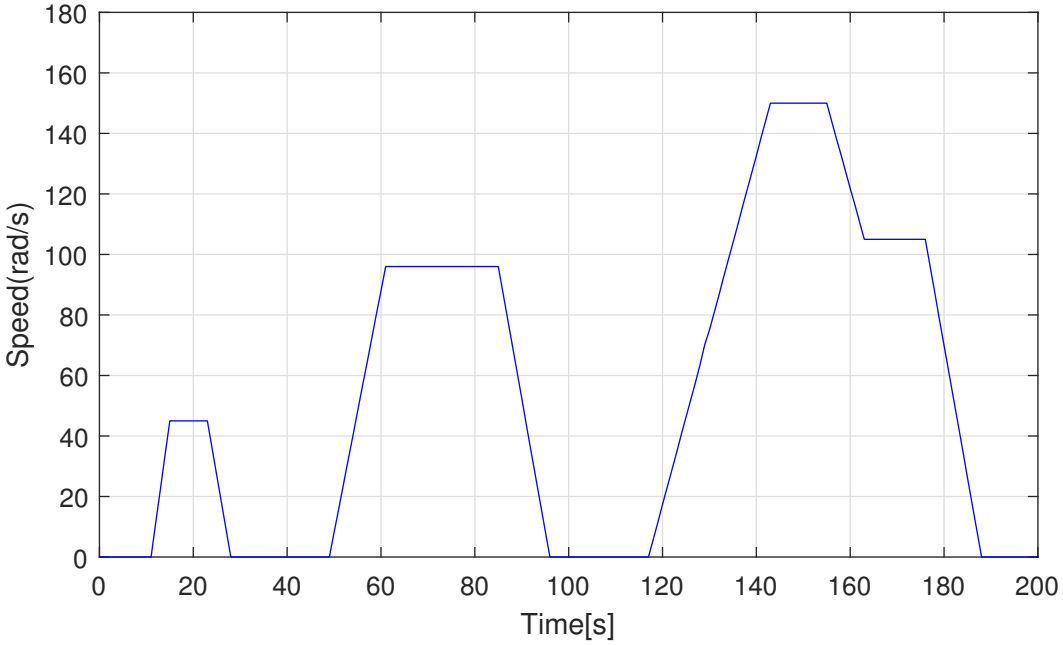


Figure 3.9: Reference speed profile for 1 kW DC motor drive

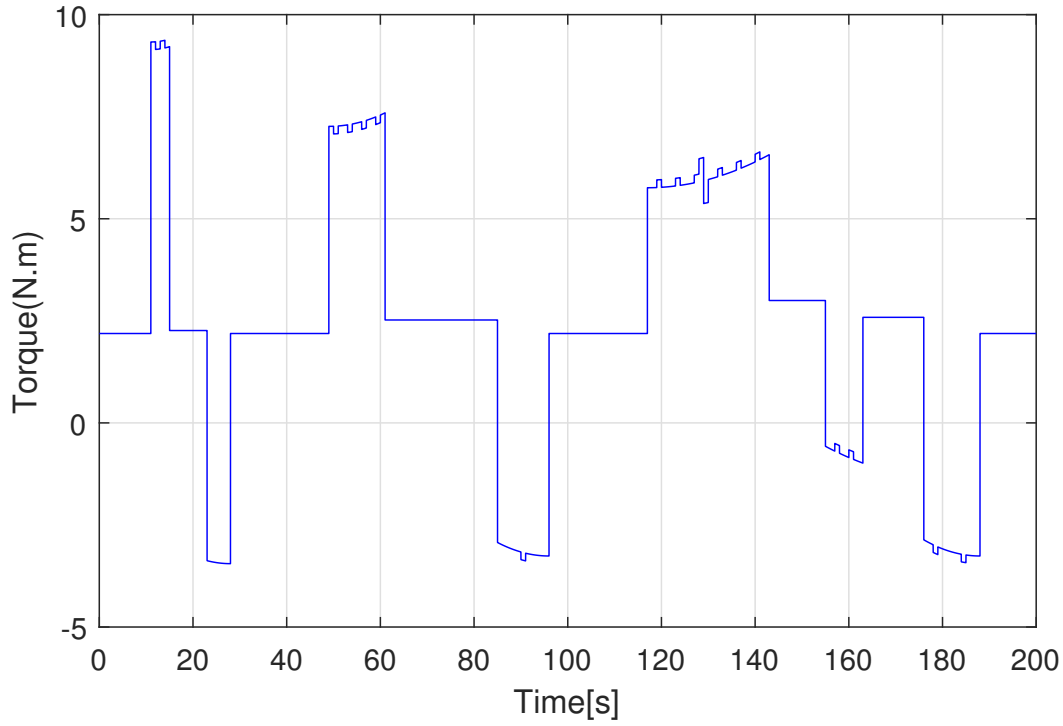


Figure 3.10: Load torque profile for 1 kW DC motor drive

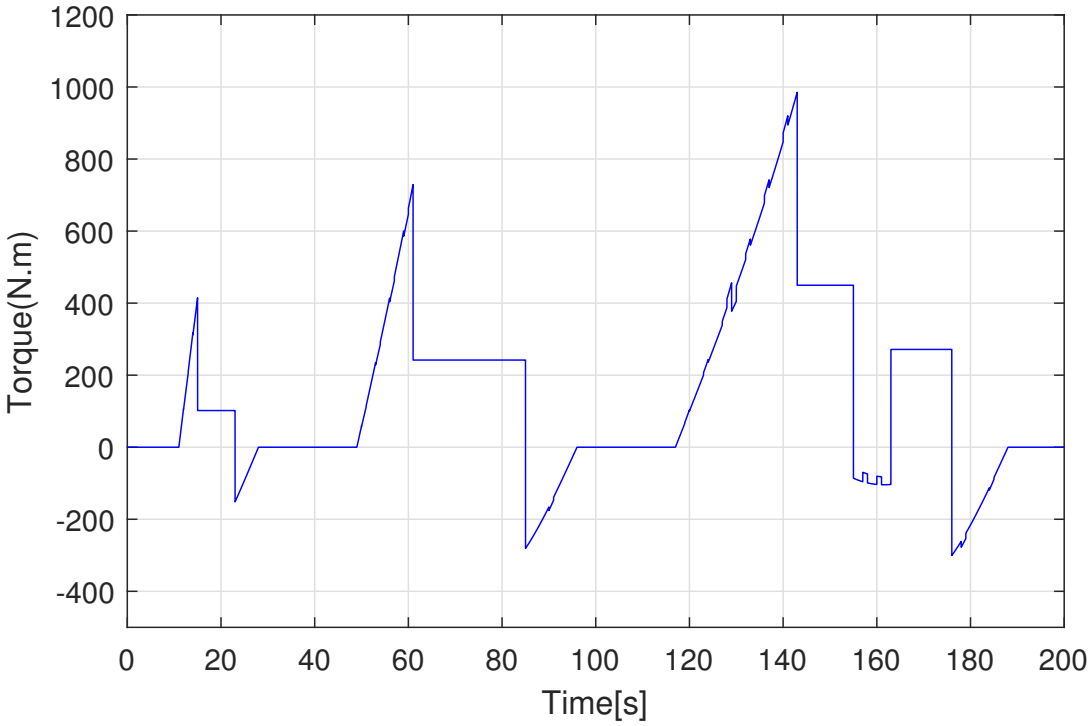


Figure 3.11: Power profile for 1 kW DC motor drive

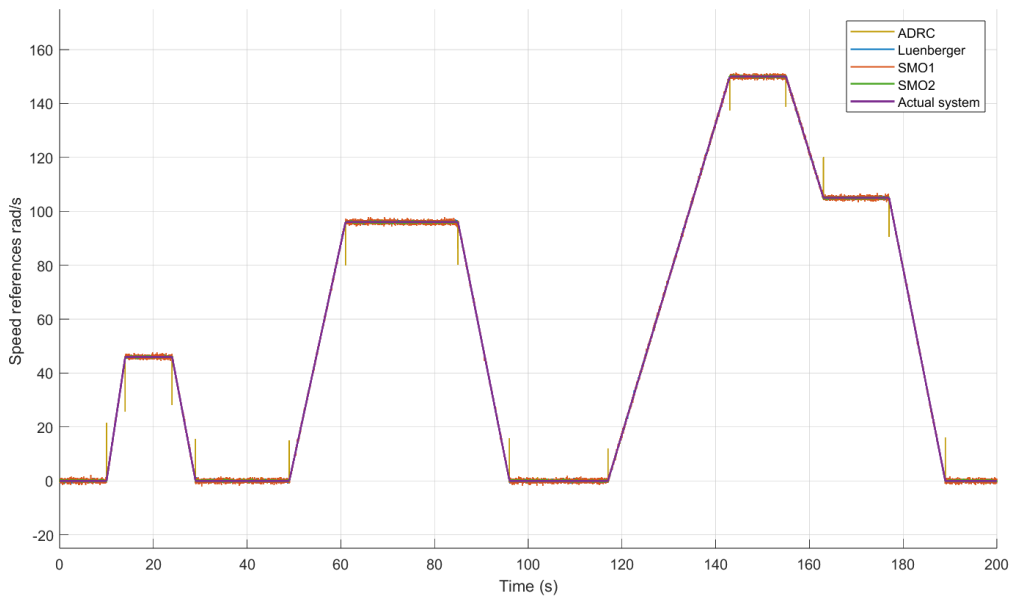


Figure 3.12: Speed Response During the Electric Vehicle Driving Cycle.

Figure 3.13 presents the load torque evolution during the same driving cycle, comparing the reference torque obtained from the vehicle dynamics model with the torque estimated by the ADRC-based observer. The estimated torque closely follows the actual load torque profile, successfully capturing rapid variations associated with transient driving conditions such as acceleration and braking.

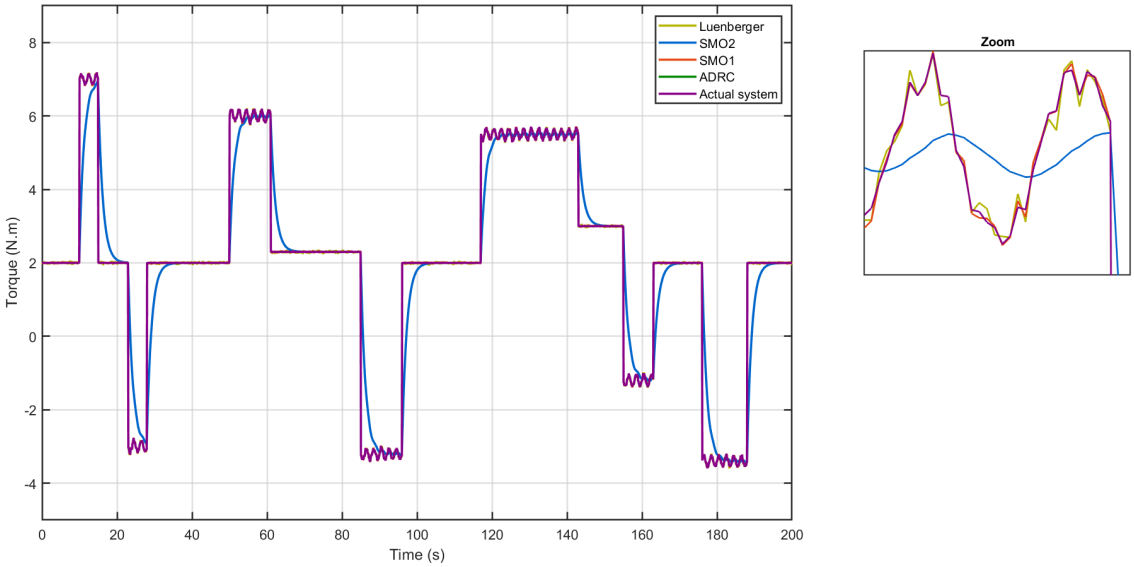


Figure 3.13: Loude Torque Response of ESO-ADRC ,SMO1 ,SMO2 ,Luenberger.

During high-demand phases such as initial acceleration, the load torque reaches peak values of approximately 12 N·m, while during steady-state cruising it stabilizes in the range of 3–4 N·m depending on vehicle speed and road resistance. In addition, during uphill operation (e.g., $\theta = 5°$), the load torque increases significantly due to the gravitational component. The observer accurately detects these variations, enabling the controller to compensate through the feedforward path. As a result, speed deviations remain minimal, demonstrating the robustness and practical effectiveness of the proposed approach for real electric vehicle operating conditions.

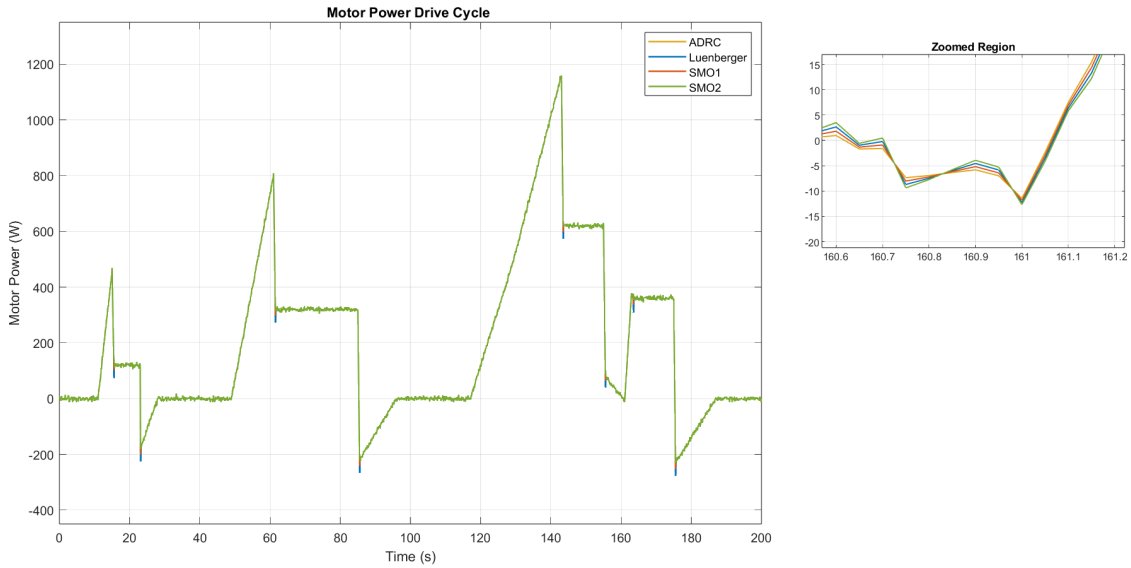


Figure 3.14: Motor Power Response During the Electric Vehicle Driving Cycle.

In the last figure 3.14 ,The four observer-based approaches produce nearly identical power responses throughout the driving cycle, demonstrating that all observers ensure similar energy delivery to the motor under normal operating conditions. However, the zoomed region highlights slight differences in transient behavior. The ADRC and Luenberger Observer exhibit smoother power transitions with reduced oscillations, whereas the SMO1 observer presents noticeable high-frequency fluctuations due to the chattering phenomenon inherent to classical sliding-mode techniques. The SMO2 observer significantly attenuates these oscillations, providing a smoother response while preserving the robustness advantages of sliding-mode estimation.

Overall, the results confirm that observer-based load torque estimation does not significantly affect the steady-state power demand of the drive system but improves transient disturbance compensation. Among the evaluated approaches, the ADRC and Luenberger Observer provide the smoothest power behavior, while SMO2 offers a satisfactory compromise between robustness and reduced chattering.

3.6 Discussion of Results

The simulation results obtained across all test scenarios consistently confirm the superior performance of the ADRC-based Extended State Observer compared with the other implemented strategies. Its ability to estimate and reject disturbances in real time without requiring precise knowledge of system parameters makes it the most suitable candidate for EV applications where load conditions vary continuously and unpredictably.

The Luenberger observer provides a reliable and computationally efficient alternative. Its linear structure simplifies gain tuning and guarantees stability under well-defined operating conditions. While it does not match ADRC in terms of disturbance rejection speed, its predictable behavior and low implementation complexity make it attractive for embedded control systems with limited computational resources.

SMO1, despite offering strong theoretical robustness guarantees, is limited in practice by the chattering phenomenon. The high-frequency switching oscillations it introduces are undesirable in a motor drive context and would require additional filtering that could compromise response speed. SMO2, based on the super-twisting algorithm, successfully mitigates this limitation and offers a satisfactory compromise between chattering suppression and estimation accuracy.

Overall, the results validate the effectiveness of observer-based torque estimation as a key enabler for advanced DC motor control in electric vehicle applications, supporting improved energy efficiency, passenger comfort, and drivetrain safety.

3.7 Conclusion

This chapter investigated the integration of load torque observers into a closed-loop DC motor drive system and evaluated their performance under realistic operating conditions. The results demonstrated that observer-based torque estimation significantly improves disturbance rejection, speed regulation, and system robustness compared with conventional PI control. Among the studied approaches, the ESO-ADRC and Luenberger Observer provided the best overall performance, while SMO1 and SMO2 offered accept-

able estimation capabilities with different trade-offs regarding chattering and transient response. Finally, the application to an electric vehicle driving cycle confirmed the effectiveness of the proposed observer-based control strategy for practical electric mobility systems.

General Conclusion

This thesis addressed the problem of load torque estimation and disturbance compensation for secure speed control in electric vehicle propulsion systems. A complete DC motor drive system was developed and combined with observer-based estimation techniques in order to improve disturbance rejection, speed tracking, and robustness under varying operating conditions.

The work began with the mathematical modeling of the DC motor and the electric vehicle propulsion system, leading to a cascaded control architecture composed of an outer speed loop and an inner current loop. This structure was chosen to ensure accurate speed regulation together with a fast torque response. Load torque variations were identified as the main source of performance degradation in the drive system, motivating the need for accurate real-time disturbance estimation.

Four observer-based techniques were then designed and studied: the Luenberger Observer, the First-Order Sliding Mode Observer (SMO1), the Second-Order Sliding Mode Observer (SMO2), and the Extended State Observer (ESO) within the Active Disturbance Rejection Control (ADRC) framework. Each observer was first evaluated under open-loop conditions to assess its intrinsic estimation behavior, before being integrated into the closed-loop drive system.

The simulation results showed that observer-based torque estimation clearly outperforms the conventional PI-controlled system, reducing speed deviations, shortening recovery time after disturbances, and improving overall robustness. The Luenberger Observer and the ESO-ADRC offered the best overall balance between estimation accuracy, disturbance rejection, and smoothness of response. SMO1 converged quickly but suffered from chattering, while SMO2 reduced this chattering effectively at the cost of a slightly slower transient response. These trends were confirmed experimentally on the test bench, where the ESO showed greater robustness than the Luenberger Observer under real disturbance and parameter-uncertainty conditions.

The proposed approach was finally validated on a realistic electric vehicle scenario using a driving-cycle-based speed reference. The results confirmed that the observer-based strategy maintains accurate speed tracking and stable operation even under continuously varying load conditions representative of real electric mobility systems.

Overall, this work shows that load torque estimation is an effective way to improve the performance, reliability, and robustness of electric vehicle drive systems, and confirms the practical relevance of observer-based disturbance compensation for advanced electric propulsion applications.

As future work, several directions can be considered: full experimental implementation

of all four observers on a real-time hardware platform, investigation of sensor faults and cybersecurity aspects in the estimation loop, integration of adaptive or intelligent (e.g., AI-based) observers, and extension of the proposed methodology to high-performance traction machines such as PMSM and BLDC motors used in modern electric vehicles.

Bibliography

[1] J. Borregaard and M. G. Fredslund, "Sliding Mode Observer-Based Load Torque Identification for PMSM Drives," Master's thesis, Department of Energy, Aalborg University, 2022.

[2] R. Wang, Z. Huang, Y. Yang, Y. Wen, and X. Sun, "A review on robust predictive control of permanent magnet synchronous motor drives: Strategies and future trends," *AIP Advances*, vol. 15, no. 11, p. 110701, 2025. https://doi.org/10.1063/5.0304727

[3] Z. Peng, C. Du, A. Zhou, L. Liu, Y. Chen, J. Chen, and Q. Peng, "Motor torque estimation and security control for electric vehicles based on parameters feature extraction," *Advances in Mechanical Engineering*, vol. 14, no. 4, pp. 1–11, 2022. https://doi.org/10.1177/16878132221090025

[4] Z. Lu, H. Fan, and D. Xu, "Load Torque Observation and Compensation for Permanent Magnet Synchronous Motor Based on Sliding Mode Observer," *Cobot*, 2024.